Universidade de São Paulo
Instituto de Física

Simulação computacional de eletrodos orgânicos

Marcela Lopes Fernandes

Orientador(a): Profa. Dra. Helena Maria Petrilli
Coorientador(a): Prof. Dr. Carlos Moysés Graça Araújo

Dissertação de mestrado apresentada ao Instituto de Física da Universidade de São Paulo, como requisito parcial para a obtenção do título de Mestre(a) em Ciências.

Banca Examinadora:
Profa. Dra. Helena Maria Petrilli (IFUSP)
Prof. Dr. Luís Tadeu Fernandes Eleno (USP - Escola de Engenharia de Lorena)
Prof. Dr. Leonardo Antonio Errico (Universidade Nacional de La Plata)

São Paulo
2023

FICHA CATALOGRÁFICA
Preparada pelo Serviço de Biblioteca e Informação
do Instituto de Física da Universidade de São Paulo

Fernandes, Marcela Lopes

Simulação computacional de eletrodos orgânicos. São Paulo, 2023.

Dissertação (Mestrado) - Universidade de São Paulo. Instituto de Física. Depto. Física dos Materiais e Mecânica.

Orientador: Profa. Dra. Helena Maria Petrilli

Área de Concentração: Física da Matéria Condensada.

Unitermos: 1. Física computacional; 2. Física do estado sólido; 3. Estrutura eletrônica.

USP/IF/SBI-053/2023

University of São Paulo
Physics Institute

Atomic scale modelling of organic electrode materials

Marcela Lopes Fernandes

Supervisor: Prof. Dr. Helena Maria Petrilli
Co-supervisor: Prof. Dr. Carlos Moysés Graça Araújo

Dissertation submitted to the Physics Institute of the University of São Paulo in partial fulfillment of the requirements for the degree of Master of Science.

Examining Committee:
Prof. Dr. Helena Maria Petrilli (IFUSP)
Prof. Dr. Luís Tadeu Fernandes Eleno (USP - Escola de Engenharia de Lorena)
Prof. Dr. Leonardo Antonio Errico (Universidade Nacional de La Plata)

São Paulo
2023

”Once upon a midnight dreary, while I pondered, weak and weary,
Over many a quaint and curious volume of forgotten lore
While I nodded, nearly napping, suddenly there came a tapping,
As of some one gently rapping, rapping at my chamber door.
“’Tis some visitor,” I muttered, “tapping at my chamber door
Only this and nothing more.”

Ah, distinctly I remember it was in the bleak December;
And each separate dying ember wrought its ghost upon the floor.
Eagerly I wished the morrow;—vainly I had sought to borrow
From my books surcease of sorrow—sorrow for the lost Lenore—
For the rare and radiant maiden whom the angels name Lenore—
Nameless here for evermore.

And the silken, sad, uncertain rustling of each purple curtain
Thrilled me—filled me with fantastic terrors never felt before;
So that now, to still the beating of my heart, I stood repeating
“’Tis some visitor entreating entrance at my chamber door—
Some late visitor entreating entrance at my chamber door;—
This it is and nothing more.”

Presently my soul grew stronger; hesitating then no longer,
“Sir,” said I, “or Madam, truly your forgiveness I implore;
But the fact is I was napping, and so gently you came rapping,
And so faintly you came tapping, tapping at my chamber door,
That I scarce was sure I heard you”—here I opened wide the door;—
Darkness there and nothing more.”

The Raven, Edgar Allan Poe

Acknowledgments

First, I would to thank God for everything He has done and given me.

I am deeply thankful to my supervisor Dra. Helena Maria Petrilli for accepting me as your master student, for all the support in all those years and for making an old dream come true. I am immensely grateful to my co-supervisor Dr. Moyses Araujo, that have welcomed me in Sweden and helped me throughout this whole master thesis; for all the insights and guidance. They both showed me how great researchers they are, and I will be forever grateful!

I would also like to thank my family that has always believed and encouraged me. They were there in all the good and difficult moments of my life, especially my parents: Reinaldo and Airinete. Additionally, I thank my boyfriend, Paulo, for all the conversations, the support and the infinite comfort that he brought me during the harsh times.

Finally, I would like to say thank you to all the people that crossed my life in these years. The PhD students and other students that welcomed me in the Physics Institute; the PhD student in Uppsala University: Rodrigo Carvalho, that was there to teach me everything I needed, to help me adapting in a new country, and also to have nice talks about food.

Abstract

Due to several environmental issues related to the high consumption of energy, the search for higher energy storage and environmentally friendly devices was necessary. The Li-ion batteries are commercially used and known for its great efficiency. However, most commercially used batteries are all inorganic. Hence, some compounds found in these batteries are harmful to the environment and hardly recyclable. In this sense, organic lithium batteries have showed to be a good alternative to the well known batteries. There are many challenges that need to be overcome for the commercially use of an organic battery. These issues are intrinsically connected to the electrochemical properties of the electrode. In this master thesis, we analyzed and simulated, at atomic level, the changes in the organic electrode properties by changing the "spectator cation" in the material structure. In order to predict the crystalline structure of the materials, we performed the genetic algorithm, USPEX, interchanged with calculations in the framework of Density Functional Theory (DFT) performed by VASP software. Furthermore, the voltage, the density of states (DOS) and the partial charge related to each lithiation step was calculated. The electrode is composed by the ligand DHT (terephthalate), lithium ions and the spectator cations (Mg^{+2}, Na^{+}, Ca^{+2}). The calculated voltages for the materials $MgLi_2DHT$, Na_2Li_2DHT and $CaLi_2DHT$, were respectively 3,59 V, 2,96 V and 2,98 V. The density of states (DOS) shows the material's reaction to receiving an electron. On the other hand, the Bader charge analysis shows the charge difference for each part of the material when compared to the other ions. Our obtained results agree with previous experimental results. Successfully, we simulated the voltage rise for the battery material with the magnesium ion, and we obtained a greater understanding of the structure and electronic properties for the studied organic electrodes.

Keywords: DFT; lithium; organic batteries; genetic algorithm.

Resumo

Com diversos problemas ambientais relacionados ao alto consumo global de energia, a busca por meios de armazenamento com maior capacidade e amigáveis ao meio ambiente se faz necessária. As baterias de Lítio são utilizadas comercialmente e conhecidas pela sua alta eficiência. Entretanto, atualmente essas baterias são totalmente inorgânicas. Ou seja, possuem compostos prejudiciais ao meio ambiente e são dificilmente recicláveis. Nesse contexto, as baterias orgânicas de Lítio têm se mostrado uma boa alternativa as baterias já existentes. Há ainda vários desafios que precisam ser superados para a comercialização de uma bateria orgânica. Esses problemas estão intrinsicamente ligados as propriedades eletroquímicas do eletrodo. Neste trabalho simulamos e analisamos, a nível atômico, as mudanças nas propriedades de um eletrodo orgânico ao se mudar o "cátion espectador" na estrutura da bateria. A fim prever a estrutura cristalina dos materiais abordados, empregamos o algoritmo genético, USPEX, intercalado com cálculos no esquema da Teoria do Funcional da Densidade (DFT) performados pelo software VASP. Posteriormente, foram calculadas a voltagem, a densidade de estados e carga relativas a cada estado de litiação do material. A bateria é composta pelo ligante DHT (terephthalate), íons de Lítio e os íons espectadores (Mg^{+2}, Na^{+}, Ca^{+2}). As voltagens calculadas para $MgLi_2DHT$, Na_2Li_2DHT e $CaLi_2DHT$ foram respectivamente 3,59 V, 2,96 V e 2,98 V. A Densidade de Estados (DOS) mostrou a ação do material ao receber um elétron. Por outro lado, a análise de carga nos mostra a diferenciação entre a carga em cada parte do material quando comparamos os diferentes íons. Os resultados obtidos condizem com resultados experimentais. Com sucesso, simulamos o aumento na voltagem da bateria com o íon de Magnésio e obtivemos um maior entendimento da estrutura e das propriedades eletrônicas dos eletrodos orgânicos aqui estudados.

Palavras chave: DFT; lítio; baterias orgânicas; algoritmo genético.

List of Figures

List of Tables

Contents

Chapter 1

Introduction

1.1 Lithium-ion Batteries

Industrialization has changed people's life and the way we see things. However, some of these changes have been harmful to the environment. Since the XX century we have seen an increase in environmental problems as: air pollution, waste of toxic elements into the nature and the use of limited elements from nature. [7] Thus, new "environmentally friendly" alternatives are needed when it comes to energy storage devices.

Given the high industrialization, the request for more efficient energy supplies also increased. It is known that energy consumption have increased exponentially from the early 1900 to the new millennium. The emerge of Lithium-ion batteries is dated from 1970s, when chemist M. Stanley Whittingham proposed titanium disulfide (TiS_2) as a cathode material. [8] From then, lithium-ion batteries showed an enormous potential due to their superior electronic properties.

Although the first studies on the electrochemical properties of lithium have been done in the beginning of the century, only after 1991 the lithium-ion battery started to be commercially used. Afterwards, lithium-ion batteries became particularly popular and many generations were developed, yet all using inorganic materials in their devices, as: $Li_xMn_2O_4$ and Li_xFePO_4. [9] [10]

In recent demand for greener technology, organic electrodes emerged as a promising and prominent alternative. Researches on organic material for batteries date 1969 [11],

but they have only been studied again recently. The huge success of the inorganic materials changed the focus of researches as inorganic batteries are more stable and offers a higher voltage. [12] [13]

Whereas prominent, many challenges need to be overcome for the use of an organic battery commercially, for instance: the energy density, storage capacity and cycle stability. On the other hand, organic batteries show many benefits; they are easily found in nature - therefore, more easily fabricated, they are flexible and can be easily recycled.[14] [15]

Computational resources and quantum calculations have been more communally used for the design of new electrode materials. Studies by Moyses *et al* [16] [17] show how computational simulations and genetic algorithms combined are used to infer different organic electrode materials. As seen in Figure 1.1, these new methods can be used to the design and discover of new organic materials.

Figure 1.1: Concept of the flow from the organic realm to the design of new material by the interpolation between quantum mechanic, data and artificial intelligence.

Organic electrodes are usually divided into two groups, being p, n or bipolar materials, depending on the charge from the redox reactions. While the p-type goes from negatively charged to neutron state, n-type goes from the neutron state to positively charged. The transition will depend if the material is an anode or a cathode. [13] [18]

The design of new organic material is crucial since new materials means cheaper and more sustainable alternatives. With the high demand for new materials Ali *et all* [2] proposed an electrode with the ligand p-DHT (2,5-dilitium-oxy)-terephthalate), the studies have been conduced with $Lix_M - p - DHT$ molecule where M stands for an

spectator cation. The spectator ions are not part of the cycling of the battery, therefore only lithium ions move during the charging and discharging of the battery as seen in Figure 1.3.

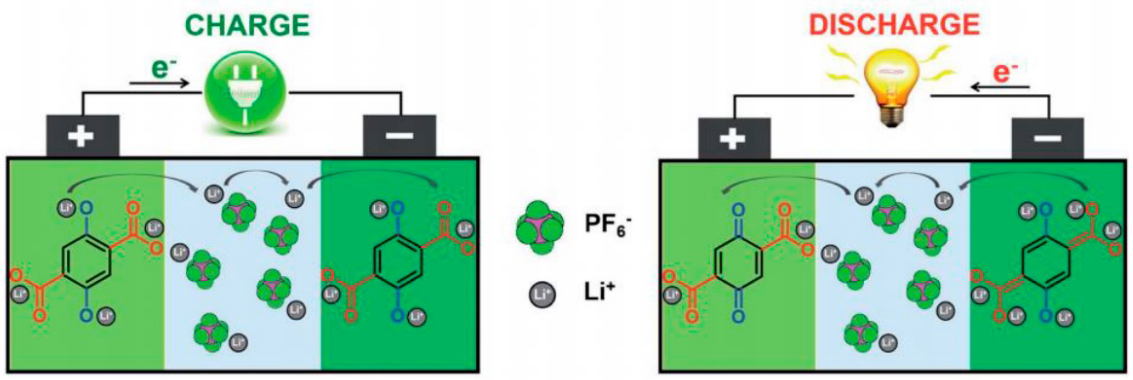

Figure 1.2: Charge and discharge schema of a lithium-ion battery with the organic electrode $Li_4 - p - DHT$ Reproduced from [1]

Ali *et al* [2] also shows how the electrode properties changes by the influence of the spectator cation. When magnesium, calcium or barium ions are within the crystalline structure of the material, changes as the electronic potential and charge distribution during cycling also happen. However, studies can not quantify and explain how these the ions effectively change in the molecular helm, and how it impacts the electronic and crystalline structure of these materials.

Therefore, the goal of this project is to have a better understanding into the organic electrodes and deal with the limitations related to the voltage profile through cation substitution.

In order to have a better understanding of the spectator cation influences, we studied three different cations: magnesium, calcium and sodium, throughout their lithiation process. Experimental results showed that the magnesium is the most prominent spectator cation, showing a voltage of 3.4 V - 800 mV more than the material without it, as it is seen in Figure 1.4 [2]. The lithiation process of the of the material without any spectator cation is given by:

$$LiDHT + 2Li + 2e^{-} \rightarrow Li_3DHT$$

While with the spectador cation is given by, as also seen in Figure **??**:

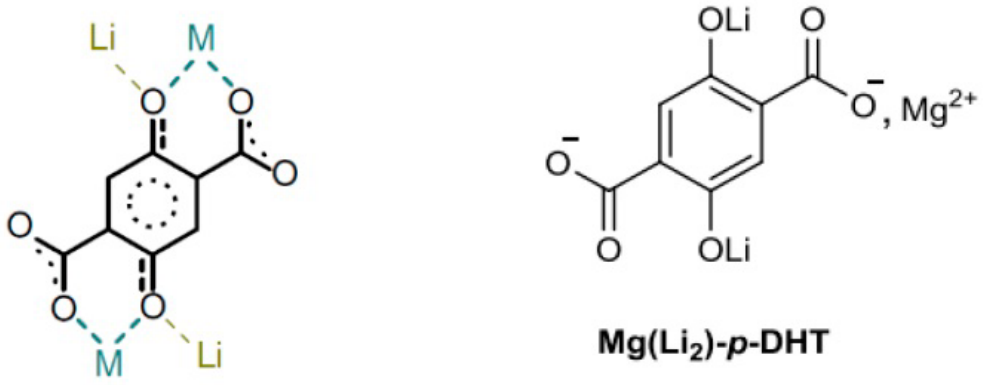

Figure 1.3: On the left: $Li_2M - p - DHT$ (2,5-dilitium-oxy)-terephthalate) molecule, being M = spectator cation. On the right: $MgLi_2 - p - DHT$ molecule. Reproduced from [2].

$$MDHT + 2Li + +2e^- \rightarrow Li_2MDHT$$

Where M = magnesium, sodium and calcium cations.

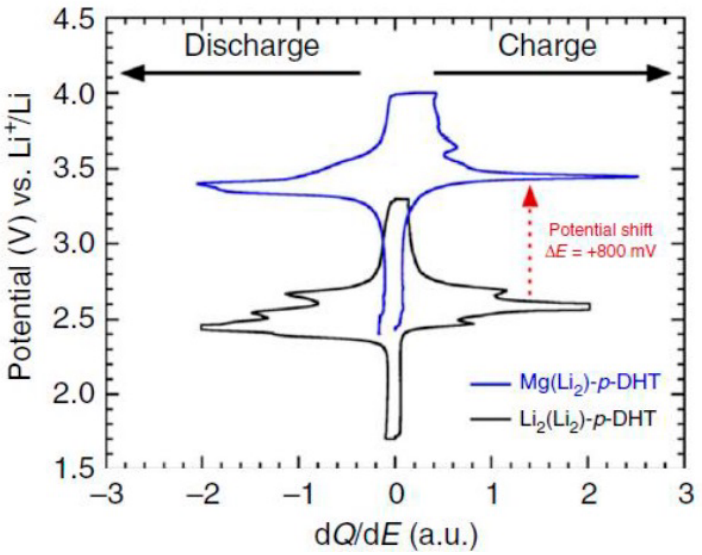

Figure 1.4: Experimental analysis of an organic electrode potential with and without magnesium as an spectator cation. Reproduced from [2]

Aiming at the simulation of the lithiation process, a crystal structure will be predicted for each lithiation step. For that, we employ DFT (Density Funtional Theory) calculations interchanged with USPEX, a genetic algorithm based software. This methodology has showed to be efficient in predicting the crystalline structures of or-

ganic electrode materials as demonstrated by Carvalho *et al.* [17]

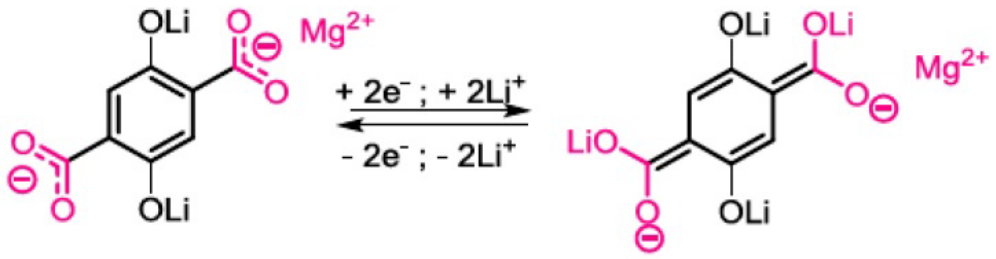

Figure 1.5: Lithiation process schema of the $MgLi_2 - p - DHT$ molecules. Intially there are 2 lithium atoms and by the end of the lithiation step, trere are 4 lithium atoms. Reproduced from [3]

Chapter 2

Methods

Since last century, many attempts have been made to solve and to have a analytical solution to the Schrodinger equation (2.1) for both molecular and solid-state systems. The challenging task of developing methods and theories for a many-body problem was partially solve by the rise of DFT (Density Functional Theory) due to its lower computational costs, when compared to the wave functions based methods. In this dissertation the framework adopted for molecules and solids calculations is the DFT. In this section we will review main theorems and concepts that forms the DFT.

As stated previously, the solution to the many-body problem starts by the Schrodinger equation:

$$\hat{H}\Psi = E\Psi \tag{2.1}$$

as the equation is describing a multi electron and nucleus system, the Hamiltonian needs to take in consideration all the interactions between the them. Therefore, the Hamiltonian is written as follows [19]:

$$\hat{H} = \hat{T}_e + \hat{V}_{ee} + \hat{T}_N + \hat{V}_{NN} + \hat{V}_{eN}, \tag{2.2}$$

where the $\hat{T}_e$ and $\hat{T}_N$ is the kinetic energy operators of the electrons and nuclei. $\hat{V}_{eN}, \hat{V}_{ee}$ and $\hat{V}_{NN}$ are the potential energy operators, being eN the electron-nucleus interaction, ee the electron-electron interaction and NN the nucleus-nucleus interaction. The extended version of the Hamilton in atomic units is written as follows:

$$\hat{H} = -\sum_{A=1}^{M} \frac{1}{2M_A} \nabla_A^2 - \frac{1}{2}\sum_{i=1}^{N} \nabla_A^2 - \sum_{\mu=1}^{N}\sum_{A=1}^{M} \frac{Z_A}{|r_\mu - R_A|} + \sum_{\mu=1}^{N}\sum_{\nu<\mu}^{M} \frac{1}{|r_\mu - r_\nu|} + \sum_{A=1}^{M}\sum_{B<A}^{M} \frac{Z_A Z_A}{|R_A - R_B|}, \tag{2.3}$$

having M_A as the nuclei mass from A, Z_A is the nuclei A charge and $\mathbf{r}$, and $\mathbf{R}$ are the electrons and nuclei coordinates. Finding an exact solution to the Schrödinger equation is an ardours task, for most of the many body problems an exact solution will not be found. In an attempt to deal with this problem, a set of approximations are made. The first one being the Born-Oppenheimer approximation.

The first step to any quantum mechanical problem is decoupling the nuclear and electronic movements. This is due to a rather simple approximation, known as the Born-Oppenheimer approximation. In fact, the nucleus mass is more than 1000 times bigger than a single electron mas. Hence, we can describe the nuclear motion as minimal when compared to the electrons motion. M Born and J.R. Oppenheimer proposed this idea in 1927 [20], they stated that due to this difference in motion we should neglect the nucleus motion as we should be able to describe the electron motion in every stationary configuration. Hence, the wave function can be written as [21]

$$\Psi(\mathbf{R}, \mathbf{r}, t) = \Theta_n(\mathbf{R}, t)\Phi_n(\mathbf{R}, \mathbf{r}), \tag{2.4}$$

where we separate the wave function into two parts, the time depended and nuclear part $\Theta_n(\mathbf{R}, t)$; and the electronic part $\Phi_n(\mathbf{R}, \mathbf{r})$. The adiabatic approximation assumes that the electron dynamics can be described in a faster away then the nuclear one. Therefore, the Schrödinger for the electronic motion is:

$$\hat{H}_e\Phi_n(\mathbf{R}, \mathbf{r}) = E_n(\mathbf{R})\Phi_n(\mathbf{R}, \mathbf{r}) \tag{2.5}$$

The extended version of the electronic Schrödinger equation is, then:

$$[\hat{T}_e + \hat{V}_{eN} + \hat{V}_{ee}]\Phi_n(\mathbf{R}, \mathbf{r}) = E_n(\mathbf{R})\Phi_n(\mathbf{R}, \mathbf{r}), \tag{2.6}$$

and the ionic equation is:

$$[\hat{T}_N + \hat{V}_{NN} + E_n(\mathbf{R})]\Theta_n(\mathbf{R}, t) = \epsilon\Theta_n(\mathbf{R}, t). \tag{2.7}$$

2.1 Density Functional Theory

The Density Function Theory arises in 1964 by the Hohenberg and Kohn [22] as an alternative to the previous Hartree Fock treatment to the many body problem. Hartree Fock attempts to treat the problem with a wave function approximation [23], describing it by a single Slater determinant. Although this method was highly used, it neglects the electron correlation. Hohenberg and Konh, therefore, develop a theory that calculates the Schrödinger equation describing first the total electronic density. In other words, the Schrödinger equation can be rewritten as a function depending on the density of the configuration.

In 1927, before DFT was idealized, Thomas and Fermi suggests an electronic density to describe the position of the electron in the atom [24] [25], introducing the concept that was later used by Hohenberg and Kohn in the DFT formulation. Furthermore, in 1964, Hohenberg-Kohn's theorems [22] rise as the DFT fundamentals.

THEOREM 1: *The external potential is directly related to the electronic density of the ground state.*

Thus, the first theorem states that the total energy state is connected to a unique density functional. The construction of the solution and all the information regarding this state shall be achieved from the electronic density. The total state energy is, then:

$$E = \langle\Psi| E |\Psi\rangle = E[\rho(\mathbf{r})] \tag{2.8}$$

where N is the total electrons number and can be evaluated as in integration of the of the density functional in the space, as seen in Equation 2.9

$$\int \rho(\mathbf{r})d\mathbf{r} = N \tag{2.9}$$

THEOREM 2: *The total energy can always be established given the electronic density. The total energy for the ground state is the minimum for the exact density.*

Therefore, the energy can be written as:

$$E[\rho(\mathbf{r})] = \langle\Phi|\,\hat{T}_e + \hat{V_{ee}} + \hat{V_{ext}}\,|\Phi\rangle = \langle\Phi|\,\hat{T}_e + \hat{V_{ee}}\,|\Phi\rangle + \langle\Phi|\,\hat{V_{ext}}\,|\Phi\rangle = F_{HK}[\rho(\mathbf{r})] + \int V_{ext}(\mathbf{r})\rho(\mathbf{r})d\mathbf{r}, \tag{2.10}$$

where $F_{HK}[\rho(\mathbf{r})]$ is the Hohenberg-Kohn functional and it is validated to all systems having n electron. The functional is not totally know due to T and V_{ee} components.

2.1.1 Kohn-Sham Equations

In an attempt to calculate the Hohenberg-Kohn functional, Kohn-Sham proposed a new methodology where the kinetic energy of the interecting electrons were replaced by the independent kinetic energy, similar to the Hartree Fock method. This simple change made it possible to carry and run calculations in chemistry and solid state physics given the development of exchange-correlation functionals. [26]

Equation 2.11 remarks Kohn-Sham definitions, the electron-electron interaction potential is now separated into two potentials: the Coulomb interaction and the exchange correlation potential [27]. Hence we write it as such:

$$E(p(\mathbf{r})) = T_e[\rho] + V_{ee}[\rho] + V_{ne}[\rho] = T_e[\rho] + V_C[\rho] + V_{xc}[\rho] + V_{ne}[\rho], \tag{2.11}$$

where, $T_e[\rho]$ is the kinetic energy, $V_{ee}[\rho]$ is the Coulomb interaction potential, $V_{xc}[\rho]$ is the exchange-correlation potential and $V_{ne}[\rho]$ is related to the interaction between the nucleus and the electron. We can then rewrite a Schrodinger-like equation as:

$$\left(-\frac{\hbar^2}{2m}\bigtriangledown^2 + \nu_R(\mathbf{r})\right)\phi_i = \epsilon_i\phi_i(\mathbf{r}), \tag{2.12}$$

which can be solved through a self-consistent approach, like the Hartree-Fock equations, as $\phi(\mathbf{r})$ are the Kohn-Sham orbitals. [28]. The universal functional can be rewritten as [19]:

$$F[\rho(\mathbf{r})] = T_R[\rho] + \frac{1}{2}\int\int \frac{\rho(\mathbf{r})\rho(\mathbf{r'})}{|\mathbf{r}-\mathbf{r'}|} + \tilde{E}_{XC}[\rho], \tag{2.13}$$

where the kinetic energy is defined being:

$$T_R[\rho] = -\frac{1}{2}\sum_{i}^{N} \langle\phi_i| \bigtriangledown_i^2 |\phi_i\rangle \tag{2.14}$$

In a simpler way, the universal functional can be rewritten as:

$$F[\rho(\mathbf{r})] = T_R[\rho] + J[\rho] + \tilde{E}_{XC}[\rho], \tag{2.15}$$

where $J[\rho]$ is the Coulomb interaction. Hence, obtaining the total energy for the functional is a simple task. Equation 2.16 shows the total energy related to the functional.

$$E_{KS[\rho]} = T_R[\rho] + \int \rho(\mathbf{r})V_{ext}(\mathbf{r})d\mathbf{r}\frac{1}{2}\int\int \frac{\rho(\mathbf{r})\rho(\mathbf{r'})}{|\mathbf{r}-\mathbf{r'}|} + \tilde{E}_{XC}[\rho] \tag{2.16}$$

The second HK theorem leads us to a variational solution to the system for the ground state energy. The solutions show:

$$V_{KS}(\mathbf{r}) = V_C(\mathbf{r}) + V_{XC}[\rho(\mathbf{r})] + V_{ext}(\mathbf{r}) \tag{2.17}$$

where,

$$V_{XC}[\rho(\mathbf{r})] = \frac{\delta\tilde{E}_{XC}}{\delta\rho(\mathbf{r})} \tag{2.18}$$

Thus, to solve the KS equations it is necessary to establish E_{XC} - the exchange-correlation functional. Several approximations have been proposed as an exchange-correlation functional. The most prominent ones being: the Local Density Approximation (LDA) [29] [30], the Generalized Gradient Approximation (GGA) [31], and the hybrid functionals, as B3LYP [32] (named after Becke for the exchange part of the functional and Lee, Yang and Parr for the correlation part of the functional).

2.1.2 Exchange and Correlation Functional

Density Functional Theory (DFT) was first introduced in the 1960s, and since then have been heavily used as a tool to describe molecules and solids characteristics as molecular geometries and ground state energies. In a small period of time, DFT has become an common alternative to Hartree Fock (HF) theory due to its greater accuracy in predicting termochemistry properties. Besides the greater accuracy, DFT calculations could be easily performed. However, scientist had a difficult time describing an "ideal" exchange correlation functional in DFT, as seen in Equation 2.19. On the other hand, Hartree Fock method has a exact exchange treatment but has no correlation being described, as written in Equation 2.20.

$$\left[-\frac{\hbar}{2m_c}\delta + V^{ion}(\mathbf{r}) + V^{el}(\mathbf{r}) + V^{XC}(\mathbf{r})\right]\phi_n(\mathbf{r}) = E_n\phi_n(\mathbf{r}) \tag{2.19}$$

$$\left[-\frac{\hbar}{2m_c}\delta + V^{ion}(\mathbf{r}) + V^{el}(\mathbf{r})\right]\phi_n(\mathbf{r}) + \int V^{X}(\mathbf{r},\mathbf{r'})\phi_n(\mathbf{r'})d^3\mathbf{r'} = E_n\phi_n(\mathbf{r}) \tag{2.20}$$

In an effort to have a better description of the exchange functional in DFT, comes the idea to use the exact exchange from Hartree Fock in the DFT approximation of the exchange correlation functional. In 1993, Becke et al. [32] achieved the goal of creating the first functional with a "Hartree Fock exchange" within the DFT approximation, which was later named a hybrid functional [33] [34].

(a) Local Density Approximation (LDA) and Generalized Gradient Approximation (GGA)

DFT is described here in terms of the Kohn Sham formulation. In Kohn Sham density functional theory the many-body Schrödinger equation is set as 2.19 where, $V^{ion}(\mathbf{r})$ is the potential due to the positively nuclei, $V^{el}(\mathbf{r})$ is the Coulomb potential and the last one, V^{XC} is the exchange correlation potential. All the formalism was well described and it all comes down to the exchange correlation potential. One of the fist and simplest approximation for the term was the "local density approximation"(LDA) [29].

LDA equation can be written as follow:

$$E_{XC}^{LDA}[n] = \int \epsilon_{XC}(n) n(\mathbf{r}) d^3\mathbf{r} \tag{2.21}$$

A better approach was to include the spin interaction into the LDA approximation, what became the "local-spin density approximation" (LSDA)[35], which has the following form:

$$E_{XC}^{LSDA}[n_\uparrow, n_\downarrow] = \int \epsilon_{XC}(n_\uparrow, n_\downarrow) n(\mathbf{r}) d^3\mathbf{r} \tag{2.22}$$

LSDA and LDA both assume a average density throughout the molecule or material. By assuming this, the exchange energy can be underestimated. The generalized gradient approximations are more accurate than LSDA and LDA because now the expansion in terms of the gradient takes into account some density fluctuation.

GGA formalism can be written as [31]:

$$E_{XC}^{GGA}[n_\uparrow, n_\downarrow] = \int \epsilon_{XC}(n_\uparrow, n_\downarrow, \bigtriangledown n_\uparrow, \bigtriangledown n_\downarrow) n(\mathbf{r}) d^3\mathbf{r} \tag{2.23}$$

The only difference in the Hartree Fock formalism is the exchange potential term in Schrödinger equation 2.20, where the potential is the exact integral of all orbitals. Therefore, hybrid functionals can be easily described as a linear combination between an exact exchange from the Hartree Fock theory and any other exchange correlation functional as LDA, LSDA and GGA. In other words, hybrid functionals are a "type" of approximations to the exchange-correlation energy among many others.

(b) Hybrid Functional: HSE06

HSE hybrid functional was first named $\omega PBEh$ [4] by J. Heyd, G. Scuseria and M. Ernzerhof, and comes from PBE0 - a improvement of the PBE exchange correlation functional. However HSE adds one more trail, the short and long range screened Coulomb potential to the exchange interaction:

$$\frac{1}{r} = \frac{erfc(\omega r)}{r} + \frac{erf(\omega r)}{r} \tag{2.24}$$

Where the first component is the short range and the second one is the long range

component.

The hybrid functional HSE is of the form:

$$E_{XC}^{\omega PBEh} = aE_X^{HF,SR}(\omega) + (1-a)E_X^{PBE,SR}(\omega) + E_X^{PBE,LR} + E_C^{PBE} \tag{2.25}$$

Figure 2.1 shows the total energies for the H-Ne atoms. These energies are being compared with PBE and PBE0. There is an underestimation of the $\omega PBEh$ while the PBE0 overestimates the values. This difference is due to the long and short range components.

Atom	Exact[b]	PBE	PBE0	ωPBEh
H	−0.500	−0.500	−0.501	−0.511
He	−2.904	−2.891	−2.894	−2.916
Li	−7.478	−7.460	−7.466	−7.496
Be	−14.667	−14.628	−14.635	−14.676
B	−24.654	−24.609	−24.617	−24.672
C	−37.845	−37.794	−37.803	−37.871
N	−54.589	−54.529	−54.540	−54.621
O	−75.067	−75.005	−75.013	−75.107
F	−99.734	−99.661	−99.667	−99.775
Ne	−128.938	−128.846	−128.851	−128.971

Figure 2.1: Total nonrelativistic energies of atoms in hartrees. A 6-311++G(3df, 3pd) basis set. Reproduced from [4].

2.1.3 PAW Method

Describing the wave function of real materials have been a challenge since DFT was first implemented. The problem relies in the accurate description of the real wave functions: they show distinct behavior when closer to the atomic nucleus. Near the nucleus, the wave function is not as smooth, exhibiting rapid oscillations; meanwhile, as farther it is from the nucleus, the smoother it becomes. Hence, the projector augmented-wave method [36] offers a clever scheme to better describe the wave function both near the nucleus and farther. In such manner, the developed method assures the efficiency in the description of the electronic density closer to the nucleus, because it is an *ab initio*

all-electron method.

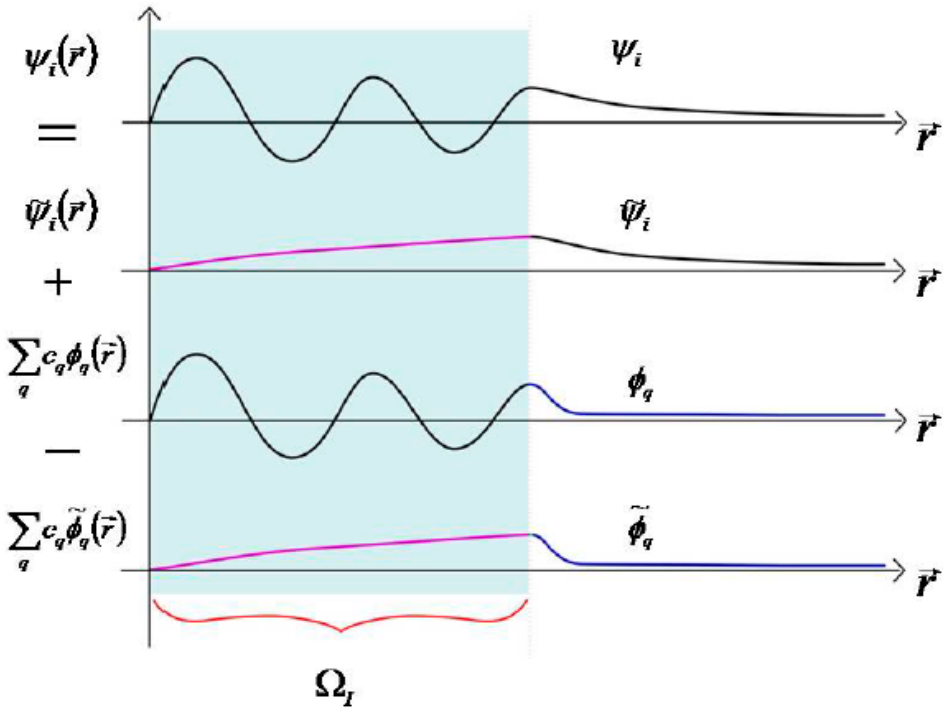

Figure 2.2: Wave function description as in Equation 2.26,where ψ_i is the total wave, $\tilde{\psi}_i$ is the PS wave function,ϕ_q is the partial wave function and $\tilde{\phi}_q$ is the PS partial wave function. Reproduced from [5]

The PAW method wave function can be written as three different functions that will be combined as one [37], as stated in Equation 2.26

$$|\psi_i\rangle = \left|\tilde{\psi}_i\right\rangle + \sum_q |\phi_q\rangle \langle\tilde{p}_q| \left|\tilde{\psi}_i\right\rangle - \sum_q \left|\tilde{\phi}_q\right\rangle \langle\tilde{p}_q| \left|\tilde{\psi}_i\right\rangle, \tag{2.26}$$

Thus, Equation 2.26 can be divided in three parts, as we can also see in Figure 2.2. The first region of the equation describes the plane waves $\left|\tilde{\psi}_i\right\rangle$ and is known as the pseudo (PS) wave function. The plane waves usually have a good description of the farther from the nucleus, therefore they serve as the post Ω_I description of the final wave function. In the other hand, the second part of the equation describes the partial all-electron functions $|\phi_q\rangle$. This part of the equation is a linear combination of the atomic functions, that said, they have a better description of the Ω_I region. Finally, the third part of the Equation is a combination of the two unwanted portions from the first two components: the plane waves in the Ω_I region and the out of the Ω_I region from the second component of the equation: that is decreasing abruptly.

2.2 Evolutionary Algorithm: USPEX

An evolutionary algorithm starts by a population of individuals in an environment with limited resources, competition for those resources causes natural selection. [6] This causes a rise in the fitness of the population. We apply a quality function to this population, and using these parameters we fit the best candidates to the next generations. When creating new generation two modifications are made to create new candidates: recombination and mutation. Recombination is a combination of two or more candidates, while mutation uses only one candidate. The evolutionary process results in a population which is increasingly better adapted to the environment. It is important to notice that during selection the best individuals are not chosen deterministically, and even weak individuals have some chance of becoming a parent of surviving. Figure 2.3, a "pseudocode", schematically shows how an evolutionary algorithm works.

```
BEGIN
  INITIALISE population with random candidate solutions;
  EVALUATE each candidate;
  REPEAT UNTIL ( TERMINATION CONDITION is satisfied ) DO
    1 SELECT parents;
    2 RECOMBINE pairs of parents;
    3 MUTATE the resulting offspring;
    4 EVALUATE new candidates;
    5 SELECT individuals for the next generation;
  OD
END
```

Figure 2.3: "Pseudocode" of the general scheme of an evolutionary algorithm. The code starts with the creation of random candidates, followed by the fitness check and selection, the creation of new combinations, evaluation of them and finally the selected candidates for the next generation. Reproduced from [6].

USPEX algorithm is a type of genetic algorithm that falls under the scope of evolutionary algorithms. The genetic algorithm was introduced in the 1970s by John Holland [38]. It is based on the evolutionary theory proposed by Darwin's works. Genetic algorithms are controlled primarily by a probabilistic strategy, just like evolutionary

patterns seeing in nature. [39] [40]

Since the first implementation, genetic algorithms were used for various purposes, from science to chess problems. USPEX stands for Universal Structure Predictor: Evolutionary Xtallography, and was developed as an alternative to the experimental methods to determine the crystalline structure of the material. It is important to highlight that experimental results are extremely import for the validation of such methods. However, USPEX and other novel software provide the ability to discover and analyse a wide range of new materials.

Most data created and analysed in this dissertation is based on the crystalline structures obtained from USPEX [38] software interchanged with the Vienna ab-initio simulation (VASP) codes [41]. First, we provided a molecule and additional chemical species to be present in the final crystalline configuration. The algorithm randomlly generates a population of 200 candidates. This population was, then, geometrically optimized and relaxed using PBE-GGA exchange correlation funtional. Next, candidates with the lowest global energy were selected to the next generation, the *ab initio* free energy of the locally optimized structures acts as the fitness function in USPEX. The following population is composed by a combination of the best candidates from the previous population, and the new candidates generated. the creation of new candidates in USPEX is made applying three different variation operators: permutation, heredity and mutation. Heredity operation is the combination of two individuals. The main information of the two individuals are taken to build a new one. The mutation transforms an candidate into a new one by changing atom position and the lattice. Finally, permutation occurs when two different atoms are exchanged. Changing the atoms positions helps finding the correct ordering.

In this study, the first generation was filled by 200 candidates; after the fitness checks, each following generation had 20 candidates selected and created from the mutation and permutation operators. The volume of each cell was calculated by USPEX and suffered variations in depending on the crystal structure. The accuracy was controlled by the E_{cut} of 600 eV and PBE-GGA exchange-correlation functionals and by default PAW basis-set. Subsequently, the final crystalline structures had their geometry optimized running a GGA calculation for all the lithiation steps with a (4 x 4 x 4) k-points and a single gamma point. Later, calculations with the hybrid function

HSE06 were run with reduced k-points and no geometrical optimization.

2.3 Thermodynamics of charge storage processes

The process of ion insertion in an electrode occurs simultaneously to the lost of the ion by the other electrode. The battery cycling is marked by the redox reactions happening simultaneously. [42] In this subsection we will briefly explore the thermodynamics of the battery cycle and explain how we connect it to the *ab initio* free energy obtained through our DFT calculations. The chemical reaction in a Li-ion battery has the Lithium ion travelling in the electrolyte from the anode to the cathode material, as it is possible to see in the mechanism below [43]:

$$\mathrm{Li_{x_0}}\mathcal{H} + (\mathrm{x_1} - \mathrm{x_0})\mathrm{Li} \rightleftharpoons \mathrm{Li_{x_1}}\mathcal{H},$$

where $\mathcal{H}$ stands for host material and $x_1 - x_0$ is the number of lithium ions the host is receiving. With our calculations we were able to estimate the free-energy of each part of this mechanism: $E(Li_{x_0})$, $E(Li_{x_1})$ and $E(Li)$. Therefore, the calculation of the Gibbs free energy for this mechanism was rather straight forward, as seen in Equation 2.27:

$$\Delta_r G(x) = E(Li_{x_1}\mathcal{H}) - E(Li_{x_0}\mathcal{H}) - (x_1 - x_0)E(Li) \tag{2.27}$$

In order to evaluate the voltage profile during the lithiation process, we calculated the voltage from the Gibbs free energy. As given in Equation 2.28:

$$V(x) = -\frac{\Delta_r G(x)}{nF} \tag{2.28}$$

The demonstration to the above equation is tied to the Nernst Equation that establishes the relationship between the cell potential in volts to the Gibbs energy. Hence, the Gibbs energy equation can also be written as Equation 2.29.

$$\Delta_r G(x) = -\frac{1}{n_{\mathcal{H}}}\frac{\partial G(x)}{\partial x} \tag{2.29}$$

Applying Equation 2.27 in Equation 2.28, we obtain the following:

$$V(x) = -\frac{\Delta_r G(x)}{nF} = -\frac{E(Li_{x_1}\mathcal{H}) - E(Li_{x_0}\mathcal{H}) - (x_1 - x_0)E(Li)}{x_1 - x_0} \tag{2.30}$$

With the use of the electronic total energy for each step, we calculated the voltage using the energy for the number of lithium-ions added in each step. The voltage was evaluated and finally we obtained the results in eV.

Chapter 3

Results

3.1 $MgLi_xDHT$

3.1.1 Crystal Structure Prediction

Crystal structure predictions are a big challenge when it comes to lithium-ion organic batteries, mostly due to the lack of experiments made in this field, the high cost that those experiments represent, and the big amount of organic materials in nature. Until this day, there are no experimental evidence of the crystal structure of the materials present in this study. Therefore all the structures studied in this project came from calculations made by this group.

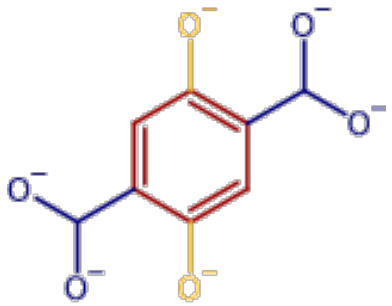

Figure 3.1: DHT molecule divided in groups by colors. In red: C_6H_2 (the aromatic ring), in blue: COO (carbon and oxigens atoms that are bounded to ring by the carbon atom) and in yellow: O (oxigens atoms directly bounded to the ring).

To predict the crystal structure, we used USPEX [38], a software based on evolutionary algorithms, interchanged with VASP (Vienna Ab initio Simulation Package) [41]. The molecules were fist modelled on Avogadro Software and later imported to

USPEX , which randomly generated an finite amount of crystals structures with the molecule and the magnesium ions. Once generated, they had the structure optimized by VASP with their internal energy as an outcome. The USPEX, then, selects the ones with lowest internal energies and generates structures applying the operators explored in Chapter 2.5 to create the next generations. Both new generated and selected structures will be again optimized by VASP and this will happen again and again until the pre-established limits are reached. This process was done for the structures with different amounts of lithium ions.

Once predicted, the structures were all relaxed (optimized) by VASP with GGA-PBE exchange-correlation functional and HSE06 exchange-correlation hybrid functional. The calculations were performed with a k-mesh 4 x 4 x 4 and an cut of energy of 400 eV.

Figure 3.2 shows the crystal structure of the delithiated phase of the electrode: MgDHT. The DHT molecule is mainly composed of carbon, oxygen and hidrogen atoms. However is import to notice that the molecule has two types of oxygen atoms: the ones connected directly to the ring and the ones bounded to the carbon atoms forming the COO^- groups. In Figure 3.1, we can see all the different groups that forms the molecules distinguished by colors. Each magnesium ion is surrounded by 6 oxygen atoms forming and octahedron geometry. It is also remarkable that two layers can been seen in the Figure, an oxide layer and an organic layer.

Figure 3.3 shows the structure predicted for the first lithiated phase. The lithium ions are now also bounded to the oxygen atoms. This bound causes a different configuration to the structure - the salt and organic layer are not as distinguishable anymore. It is important to notice that inside each unit cell there are two molecules and two magnesium atoms, therefore by adding one lithium atom per molecule, we add two lithium atoms in the cell.

Adding an extra lithium atom to the previous structure gives an extra complexity to the material, as we can see in Figure 3.4. Although the number of lithium atoms increased and more ions are bounded to the oxygen atoms, the magnesium atoms - in this configuration - still keeps the octogenarian configuration being surrounded by 6 oxygen atoms as in the delithiated phase. Lithium atoms have one valence electron. This extra electron is possibly populating π orbitals from the aromatic ring carbons,

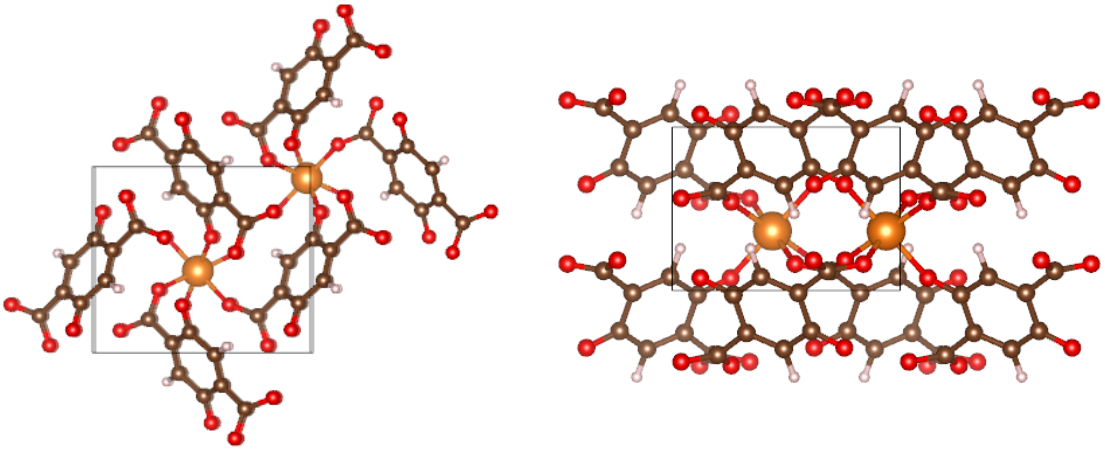

Figure 3.2: Predicted crystal structure for delithiated phase of $MgDHT$. The orange atoms are magnesium atoms, the brown ones are carbon atoms, the red ones are oxygen atoms and the white ones are hydrogen atoms.

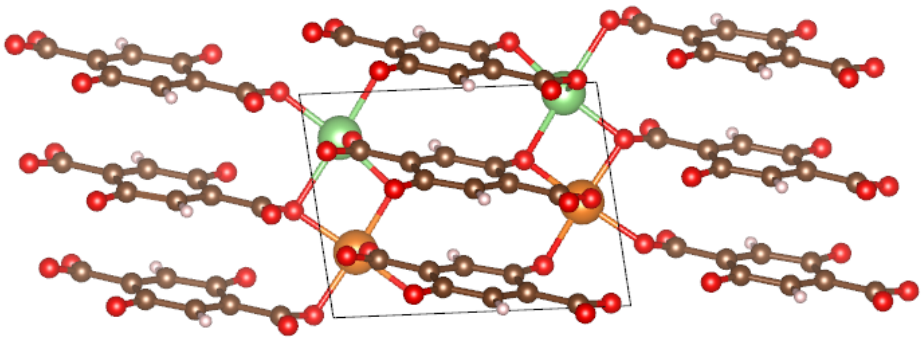

Figure 3.3: Predicted crystal structure for fist lithiated phase of $MgLiDHT$. The orange atoms are magnesium atoms, the brown ones are carbon atoms, the red ones are oxygen atoms, the white ones are hydrogen atoms, and the green ones are lithium atoms.

reducing the aromacitcity of the carbon ring. As we will see further, this is confirmed by the Density of States and Bader Analysis of the lithiated phases.

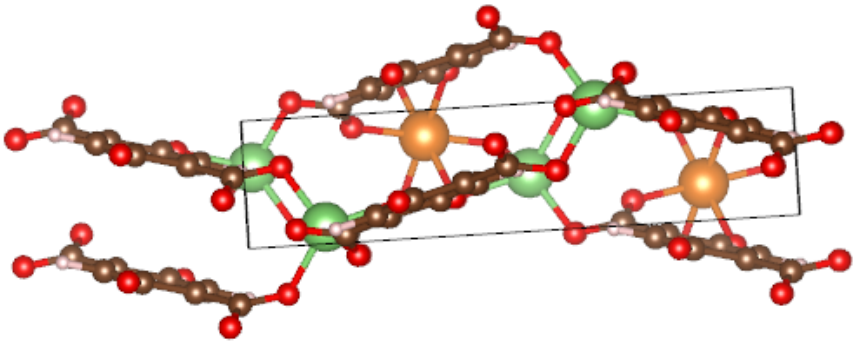

Figure 3.4: Predicted crystal structure for second lithiated phase of $MgLi_2DHT$. The color scheme is as in Figure 4.2

In Figures 3.5 and 3.6, we continued the lithiation by adding one lithium per molecule at time. We can see that now we find a total of 3 and 4 lithium per molecule in Figures 3.5 e Figure 3.6, respectively. Although more complex, we are still able to see organic and salt layers in the structures. Now, more lithium atoms are bounded to oxygen atoms from both groups O^- and COO^-, these charged states are expected to happen after the lithiation - once both a lithium-ion and an electron is introduced into the electrode material . We, thus, expect that the negative charge in those groups are higher as they are more lithiated.

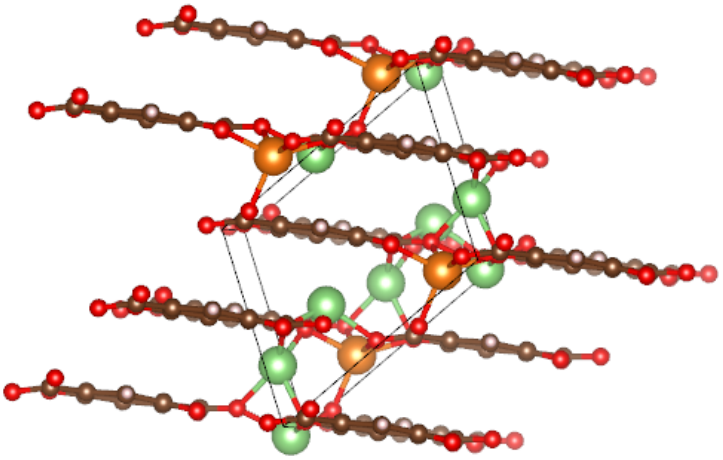

Figure 3.5: Predicted crystal structure for third lithiated phase of $MgLi_3DHT$. The color scheme is as in Figure 4.2

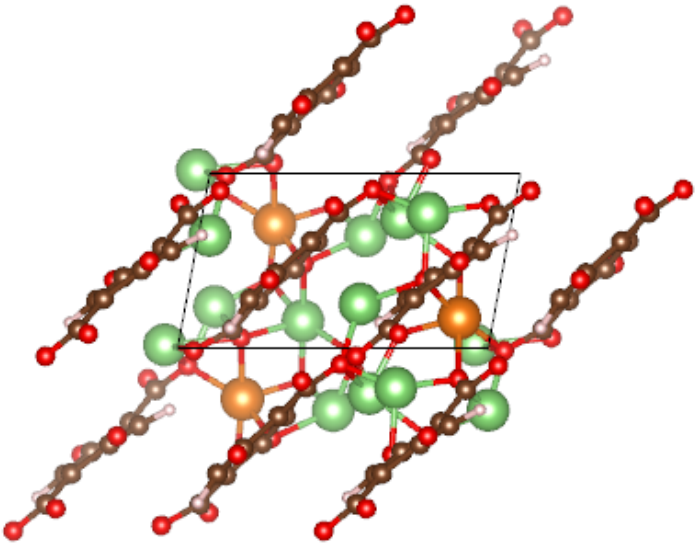

Figure 3.6: Predicted crystal structure for fourth lithiated phase of $MgLi_4DHT$. The color scheme is as in Figure 4.2

3.1.2 Voltage Profile

Experimentally, the magnesium atom as an spectator cation increases the electrode voltage. To better understand how the atom affects the material, we need to calculate the voltage for the structures found previously during the lithiation process. The voltage is calculated as indicated in Chapter 2.3. Briefly, we obtained the internal energy for each one of the structures, with this energy we could calculate the voltage for each step of the process. Experimentally, the electrode, without the spectator cation - $LiDHT$, shows a 2.6 V voltage. The chemical reaction that describes the lithiation process for the non-magnesium electrode is:

$$LiDHT + 2Li^+ + 2e^- \rightarrow Li_3DHT$$

We preformed DFT calculations with different exchange-correlation functionals to describe the system. Initially, we used PAW method with GGA-PBE as a exchange-correlation functional, further we used the hybrid functional HSE06.

The calculated voltage for the lithiation steps are showed in Table 3.1. One can see two different potential rages. The first, cathode potential, where the quinone oxygens are reduced with voltages above 3 V. The second, where the carboxylic oxygens are reduced at voltages below 1V. For the next lithiation process, the calculated voltage

was approximately 3.10 V with GGA-PBE exchange correlation potential, whereas it was an average of 3.59 V using the hybrid function, for the first and second lithiation step:

$$MgDHT + 2Li^{+} + 2e^{-} \rightarrow MgLi_2DHT$$

Steps of lithiation	Voltage (V) with GGA-PBE	Voltage (V) with HSE06
1 lithiation	3.17	3.81
2 lithiation	3.09	3.37
3 lithiation	0.67	0.53
4 lithiation	0.43	0.64

Table 3.1: Voltage values in Volts(V) calculated with different methods.

However, on Table 3.2 the same lithiation process shows an average voltage of approximately 3.55 V, for the first two lithiation steps. This value agrees more with the experimental value of 3.4 V. On both Tables 3.1 and 3.2 we see a drop in voltage on the third lithiation step. For instance, on Table 3.2 the second lithiation step shows a voltage of 3.29 V and the third lithiation step shows a 0.6 V voltage. This drop indicates that the material can be used as both an cathode and an anode.

Steps of lithiation	Voltage (V) with HSE06 + geometry optimization
1 lithiation	3.80
2 lithiation	3.29
3 lithiation	0.60
4 lithiation	0.64

Table 3.2: Voltage values calculated with crystal structure optimized with HSE06 hybrid functional

3.1.3 Electronic Structure

Aiming to gain insights on how the lithiation process works as the lithium-ion and an electron is inserted into - and changes - the electrode material, we calculated the

projected density of states (DOS). On the left side of every DOS Figure, one can find the normalized density of states. Previously, analysing the structures and bonds formed on each step, we inferred that probably the extra electron was populating the aromatic organic ring, breaking the double carbon bonds. Analysing Figure 3.7, we see that the first band to be popularized is the resulting hybridization between the groups C_6H_{12}, O^- and COO^-, but mostly the C_6H_{12} and O^-, which confirm our fist insight. Furthermore, on the left side we can see that, although the aromatic ring is the biggest part of the molecular orbital, when normalized, the oxygen atoms from O^- group, have a higher pick in the normalized band, thus the the oxygen atoms are more negatively charged then the carbon atoms from the ring.

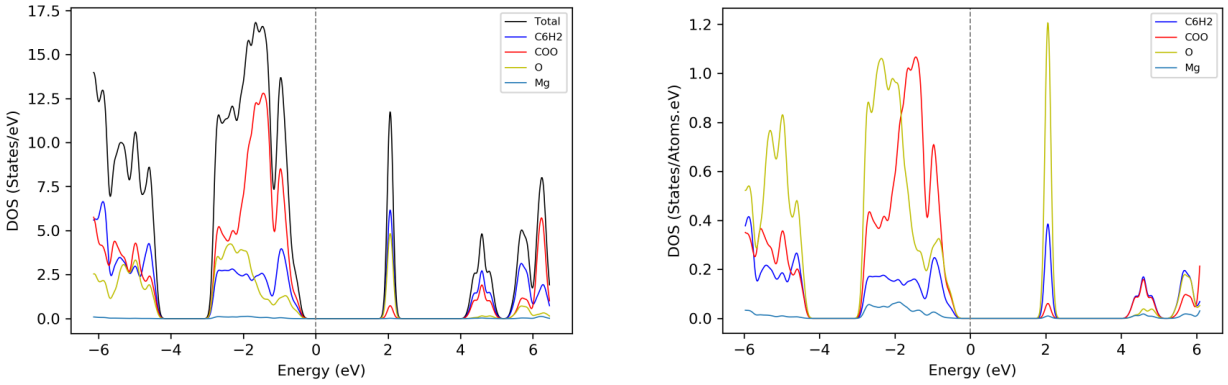

Figure 3.7: On the left: Density of States (DOS); on the right: Normalized Density of States (nDOS), of the delithiated phase $MgDHT$.

Figure 3.8 shows the density of states of the molecules after the insertion of one electron, we see then that the first band after the Fermi energy from Figure 3.8 is now half filled, as half of the band is found under the Fermi energy. Going further, on Figure 3.9, we find that after the insertion of two electrons, the first band is now totally filled. Therefore, we can confirm that in the two first lithiation steps, the electrons populate both the ring and the oxygen atoms from the O^- group.

Surprisingly, on Figure 3.9 the next band to be filled is the resulting hybridization of COO^- and C_6H_{12} groups. Moreover, we see no O^- participation in the hybridization, that shows that now the atoms being reduced are the oxygen atoms from the COO^- and it suggests that the electrons transferred to the molecule still tends to delocalize

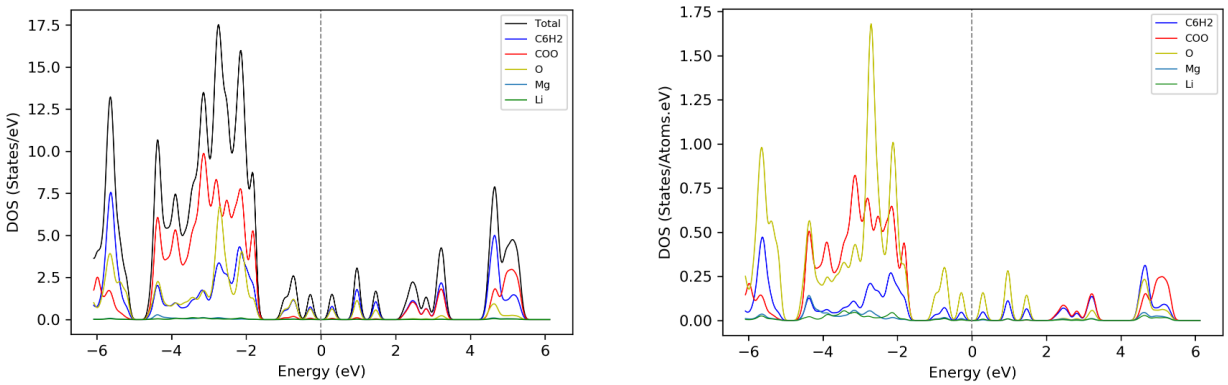

Figure 3.8: On the left: Density of States (DOS); on the right: Normalized Density of States (nDOS), of the delithiated phase $MgLiDHT$.

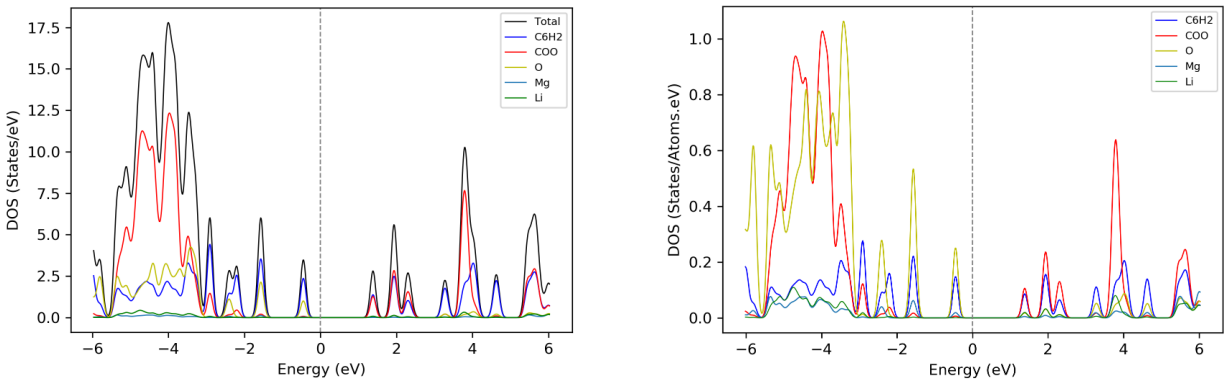

Figure 3.9: On the left: Density of States (DOS); on the right: Normalized Density of States (nDOS), of the delithiated phase $MgLi_2DHT$.

over the organic ring, besides being centered on the oxygen atoms. Something similar to the last analysis happens to the next lithiation steps - by inserting one more electron, we see in Figure 3.10, that half the band is now filled; and inserting one more electron (as in Figure 3.11), the band is now totally filled. It is import to notice that this change in the redox center happened at the same lithiation step as the voltage drop. It suggests that the oxygen atoms from the O^- have a higher redox activity and plays a big role at the increase of the electrode voltage.

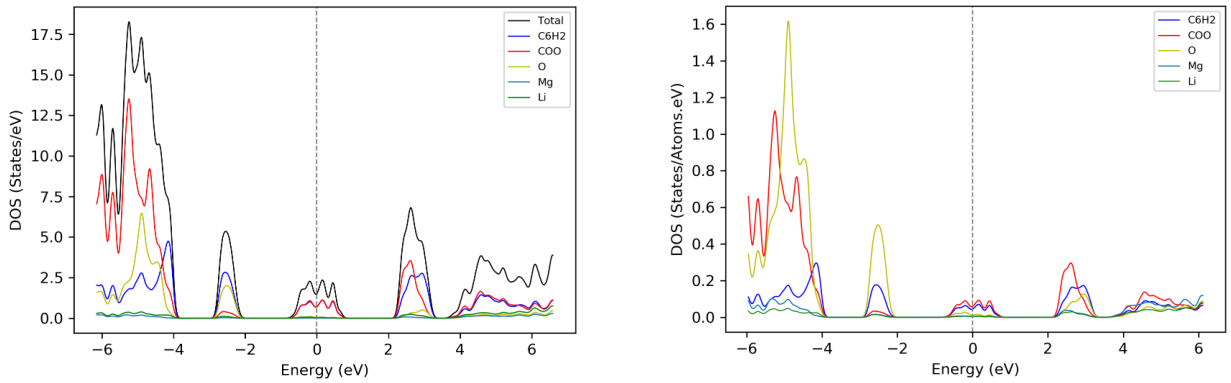

Figure 3.10: On the left: Density of States (DOS); on the right: Normalized Density of States (nDOS), of the delithiated phase $MgLi_3DHT$.

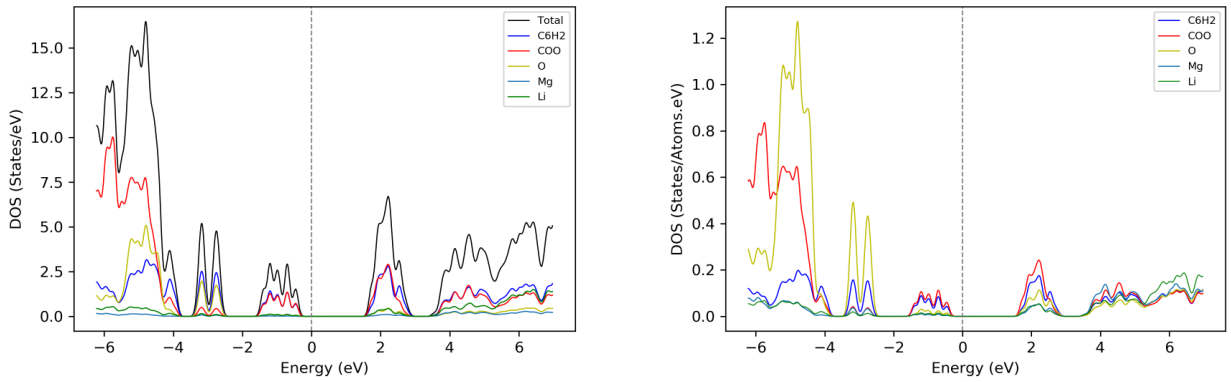

Figure 3.11: On the left: Density of States (DOS); on the right: Normalized Density of States (nDOS), of the delithiated phase $MgLi_4DHT$.

On Figures 3.12 and 3.13, we can see the integrated band that received the extra electron, or the molecular orbital that received the extra electron. The results shown are in agreement with the DOS. On the left of Figure 3.12, that shows structure $MgLiDHT$, we see that the electron is delocalized mainly in oxygen atoms of the

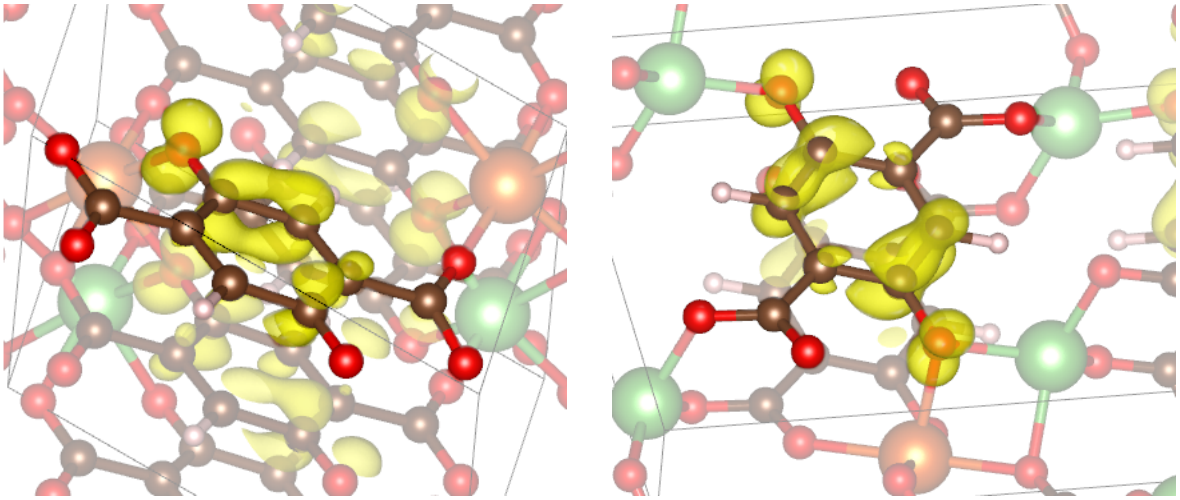

Figure 3.12: On the left: Charge density of the extra electron for $MgLiDHT$; on the right: Charge density of the extra electron for $MgLi_2DHT$.

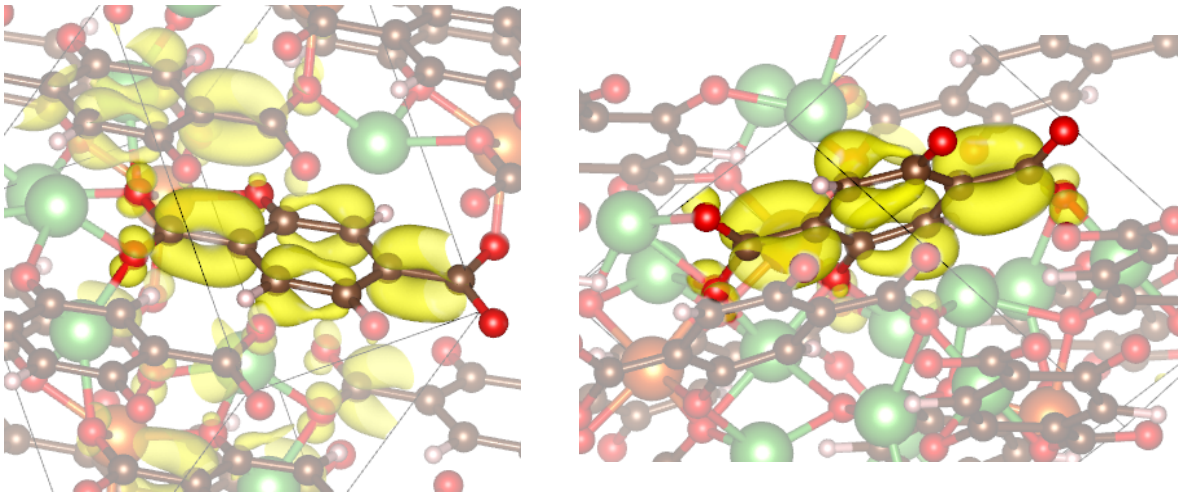

Figure 3.13: On the left: Charge density of the extra electron for $MgLi_3DHT$; on the right: Charge density of the extra electron for $MgLi_4DHT$.

O^- group, and breaking what was once a double bound in the organic ring. On the right side of the same Figure, we see that by adding one more electron, the electrons are now delocalized over both oxygen atoms and the organic ring. We see, therefore, that the organic ring during all lithiation process is acting as an electron reservoir.

Moreover, on Figure 3.13 the electrons are now delocalized over not only the organic ring but over the carbons and oxygen atoms of the COO^- group. It is import to notice that differently from the first lithiation steps, the electron localized in the COO^- group is not only localized in the oxygen atom, but also populating the carbon π bound. Therefore, the oxygen atoms from both groups have different redox potentials and thus show different voltage when populated.

3.1.4 Bader Charge Analysis

The bader charge analysis is a quantitative approach to the conclusions that we have so far about the the electron delocalization in the molecule. The analysis consists of calculating the charge in every atom of the structure, so we have not only a total charge on the molecule but also the negative charge in every part of the molecule. We organized the charge using the same division as we have been using during all the results: by diving the molecule in groups. Thereby, here we are only analysing the additional negative charge throughout the lithiation process, and not the total charges of each part of the molecule.

On Figure 3.14, on the x-axis, we have the lithation steps - being "0" the delithiated structure, $MgDHT$. The charge is constantly increasing in the C_6H_2 group, in agreement with the electronic studies. On the other hand, until the second lithiation the electronic charge is being concentrated on the ring and the O^- group, and after the sencond lithiation, the charge on the COO^- group increases dramatically, being compared to the charge stored in the organic ring.

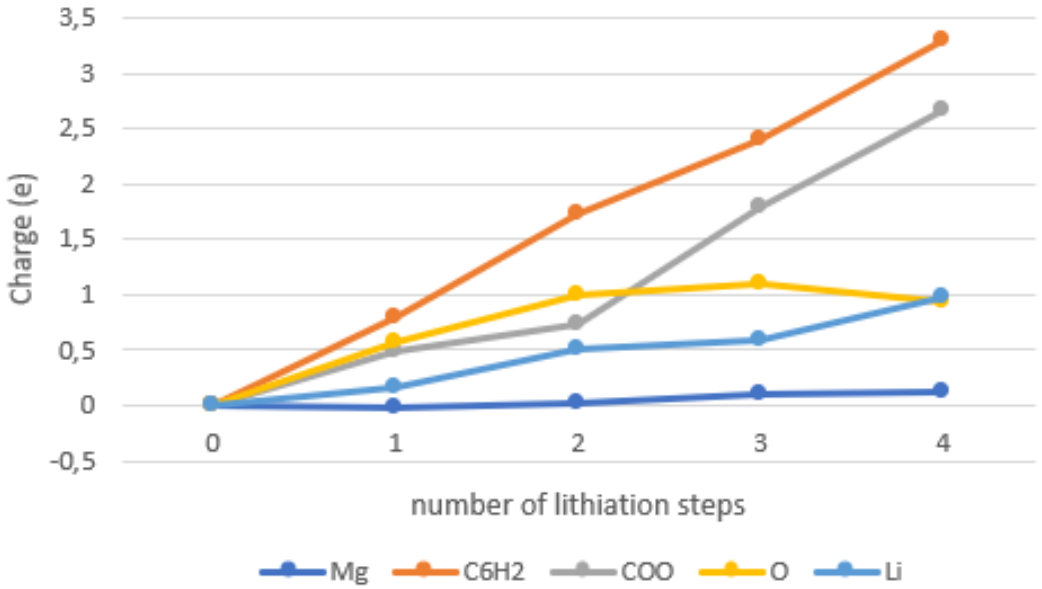

Figure 3.14: The Bader analysis results show a charge variation of each group present in the molecule as a function of the lithiation steps of the electrode.

3.2 $CaLi_xDHT$

3.2.1 Crystal Structure Prediction

We then applied the same methodology and analysis for both Calcium and Sodium as an spectator cation. As previously, we predicted the crystalline structure using USPEX interchanged with VASP, for the DFT calculations. Furthermore, we analysed how the crystalline structure changes as the lithiation process occur and we were able to calculate and simulate the voltage and the electronic structure of the materials. As we are more interested in the first two lithiation, from now own, we are only analysing the fist and second lithiation process, so we can compare to the structure having a magnesium atom.

Figure 3.15 shows the delithiated phase of the material. We see that structure wise, it is really similar to the $MgDHT$ crystalline structure. Having said that, we see that the Calcium atom is the center of an octahedron geometry, surrounded by the oxygen atoms form the two distinct groups defined before. Due to the similarities, we expected that by inserting a extra lithium-ion and an electron into the structures, the material would show the same effect on their geometry.

Although different, Figures 3.16 and 3.17 shows that during the first and second lithiation process, we still have well defined salt and organic layers. And, as we have seen before, the atoms lithium atoms are now bounded to the oxygen atoms in both structures.

3.2.2 Voltage Profile

We can describe the lithiation process for the structures as:

$$CaDHT + 2Li^{+} + 2e^{-} \rightarrow CaLi_2DHT$$

To determine the voltage for the lithiation process, we fist performed DFT calculations with both GGA-PBE and HES06 exchange-correlation functionals. Finally, we found an average calculated voltage of 2.98 V during this double step lithiation process. Experimental results shows a 2.9 V voltage, in great agreement with our calculated result with no experimental input.

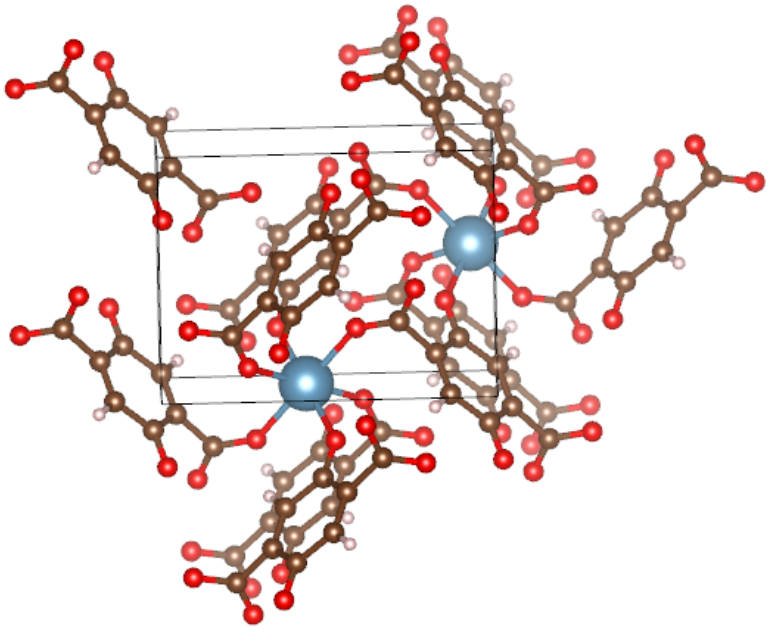

Figure 3.15: Predicted crystal structure for delithiated phase of $CaDHT$. The blue atoms are calcium atoms, the brown ones are carbon atoms, the red ones are oxygen atoms, the white ones are hydrogen atoms.

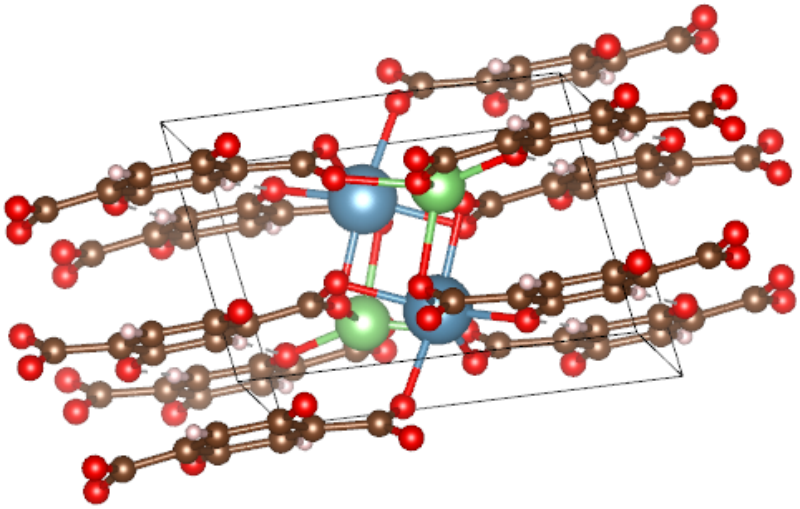

Figure 3.16: Predicted crystal structure for fist lithiated phase of $CaLiDHT$. The blue atoms are calcium atoms, the brown ones are carbon atoms, the red ones are oxygen atoms, the white ones are hydrogen atoms, and the green ones are lithium atoms.

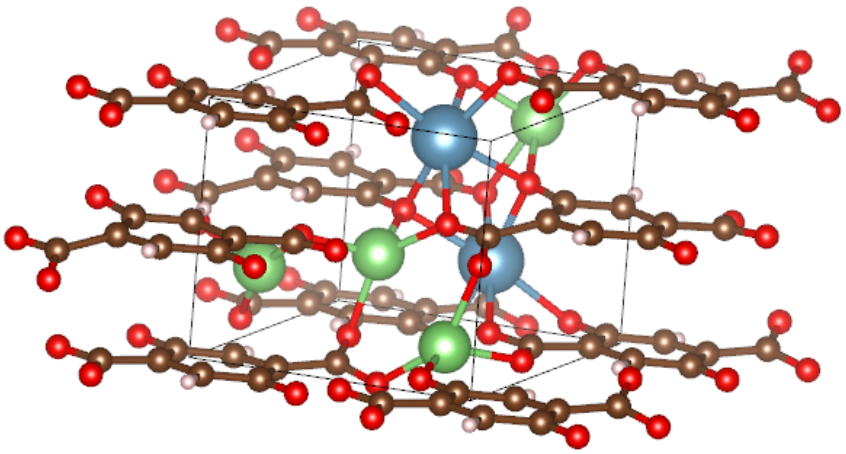

Figure 3.17: Predicted crystal structure for second lithiated phase of $CaLi_2DHT$. The color scheme is as in Figure 4.17

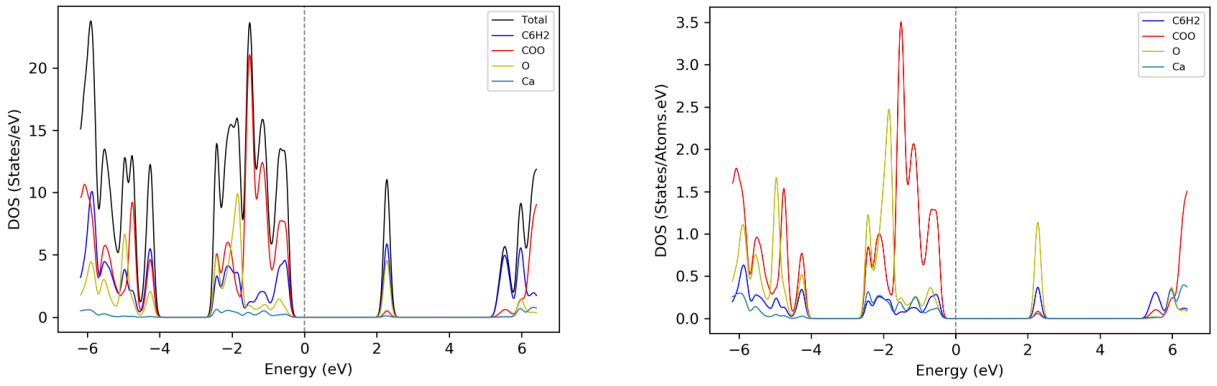

Figure 3.18: On the left: Density of States (DOS); on the right: Normalized Density of States (nDOS), of the delithiated phase $CaDHT$.

3.2.3 Electronic Structure

The electronic structure is studied through the DOS in order to elucidate the mechanism acting in the lithiation process. Figure 3.18 shows a localized band after the fermi level. This band then receives the two electrons. We see that this band is also the hybridization from the O^-, COO^- and C_6H_2 groups, but we still do not know quantitatively how much each of the groups contributes to the band. Therefore, we can only assume that, as we seen happening for the magnesium atom a spectator cation, the first two lithiation steps will populate mostly the organic ring and the oxygen atoms from the O^- group. Once again, the ring is acting as an electron reservoir. Figure 3.20 agrees with our previous result and shows the integrated band that received the electron in the lithiation process, the charge density clearly shows that the electron is delocalized over the oxygen atoms of O^- and over the ring. Although we could see contributions of the COO^- group to the vacant band, the charge density does not show that, what make us believe that the contribution from the COO^- group to the band is small.

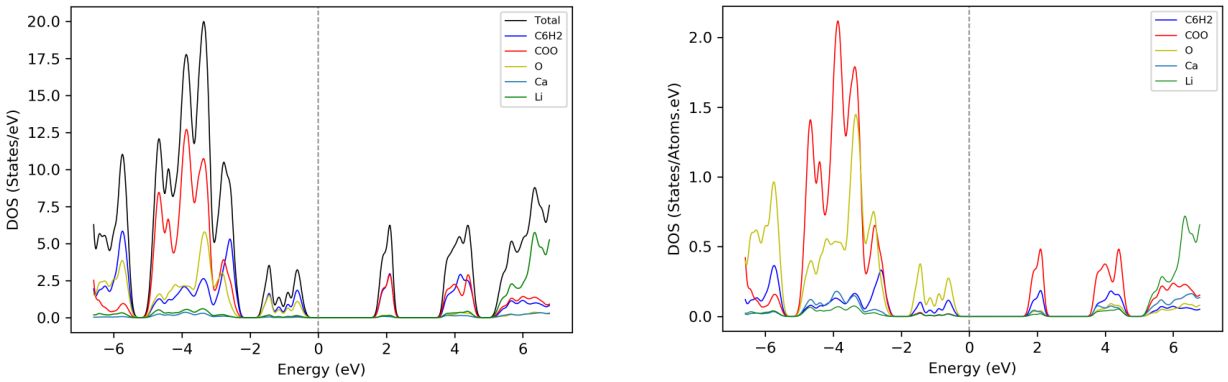

Figure 3.19: On the left: Density of States (DOS); on the right: Normalized Density of States (nDOS), of the $CaLi_2DHT$.

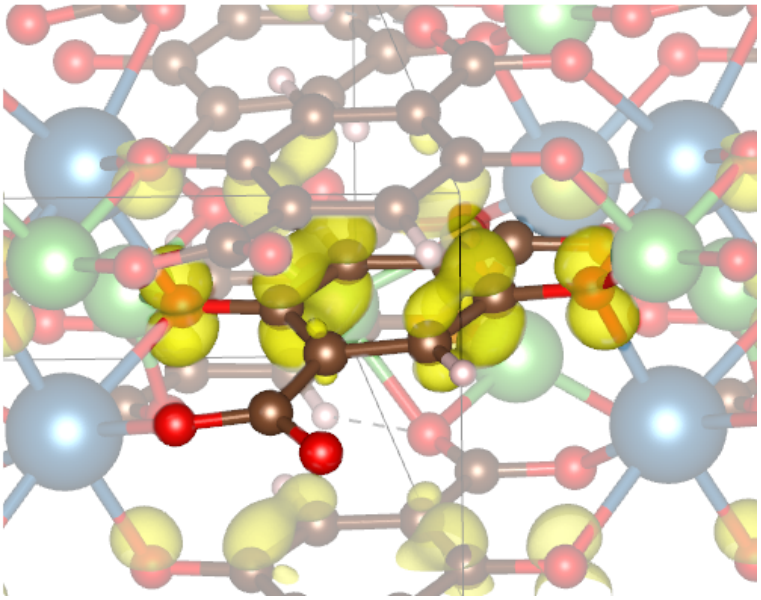

Figure 3.20: Charge density of the extra two electrons for $CaLi_2DHT$

3.2.4 Bader Charge Analysis

Similar to our previous Bader Analysis for the magnesium atom as a spectator cation, we had a charge calculation by VASP that was later treated by the code provided by Tang *et al* [44], which has showed us numerical values for the localized charge on each atom. These numerical values were added in the relative molecule groups and plotted as in Figure 3.21. We can see, on the x-axis, the lithation steps - being "0" the delithiated structure, $CaDHT$. Moreover, here we only represent the charge difference from the delithiated structure to the second lithiation step. As expected from the Bader analysis for the crystal with the magnesium atom, the charge is constantly increasing in the C_6H_2 group, also in agreement with the electronic studies. On the other hand, it is notably that the COO is now the group that has more concentrated charge during the lithiation, leaving the O group in third place when it comes to the charge distribution. Therefore, the calcium atom in fact not only changes the internal energy, and consequently, the redox potential of the material, but also changes the redox center of the molecule.

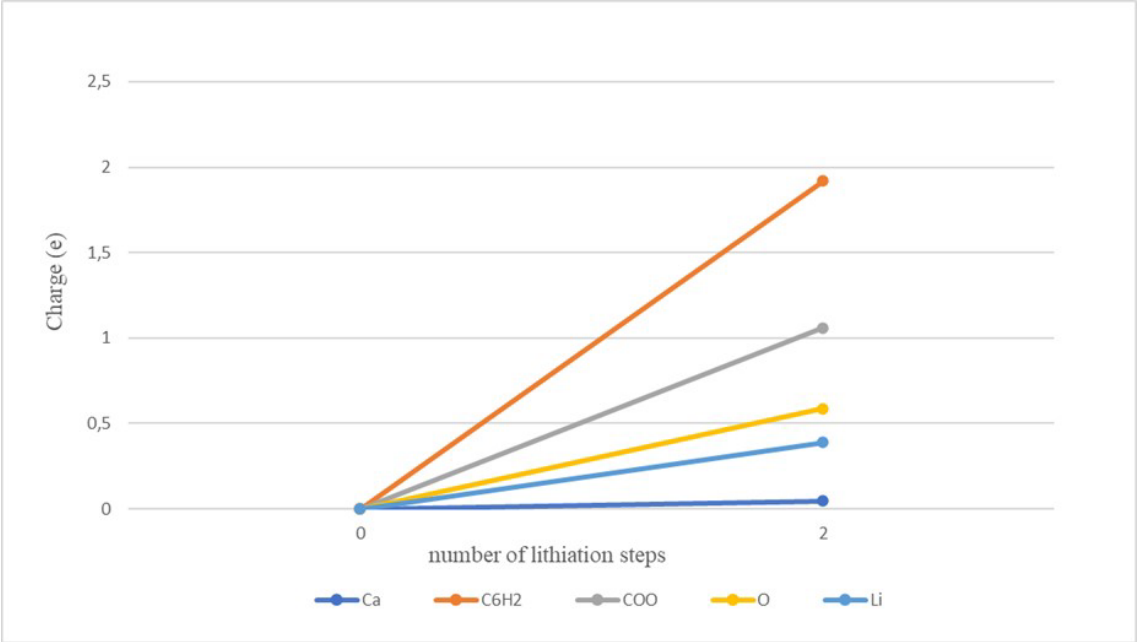

Figure 3.21: The Bader analysis results show a charge variation of each group present in the molecule as a function of the lithiation steps of the electrode.

3.3 Na_2Li_xDHT

3.3.1 Crystal Structure Prediction

First, it is important to notice that having the Sodium atom as a spectator cation alters the amount of spectator cations presented in a cell. Both sodium, magnesium, and calcium ions have positives charges, but sodium-ions are monovalent, while the other two are divalent. Therefore, to maintain a neutral molecule we needed to have two sodium ions per molecule. The amount of ions brings changes to the crystalline structure analysed. We see in Figure 3.22 that the delithiated phase shows well divided organic and salt-like layers - something we have also seen in the previous crystalline structures. Adding one lithium atom per molecule does not contribute to significantly changes on the crystalline structure: we can still see well defined layers in 3.23. However, adding more lithium atoms notably changes the structure, as seen in 3.24, where the layers are not as defined and the lithium atoms are more spreed in the structure.

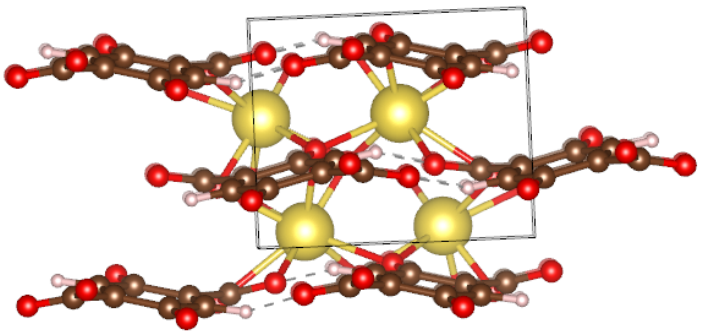

Figure 3.22: Predicted crystal structure for delithiated phase of Na_2DHT. The yellow atoms are sodium atoms, the brown ones are carbon atoms, the red ones are oxygen atoms, the white ones are hydrogen atoms.

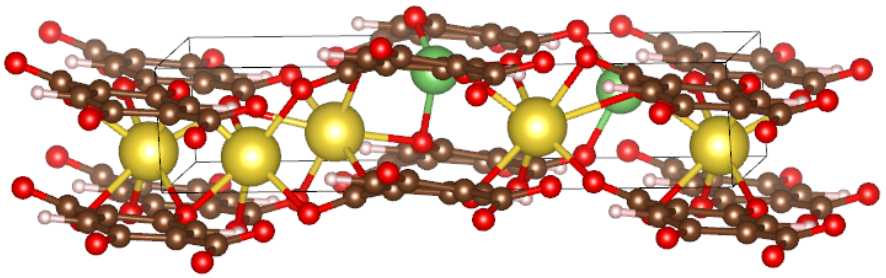

Figure 3.23: Predicted crystal structure for fist lithiated phase of Na_2LiDHT. The yellow atoms are sodium atoms, the brown ones are carbon atoms, the red ones are oxygen atoms, the white ones are hydrogen atoms, and the green ones are lithium atoms.

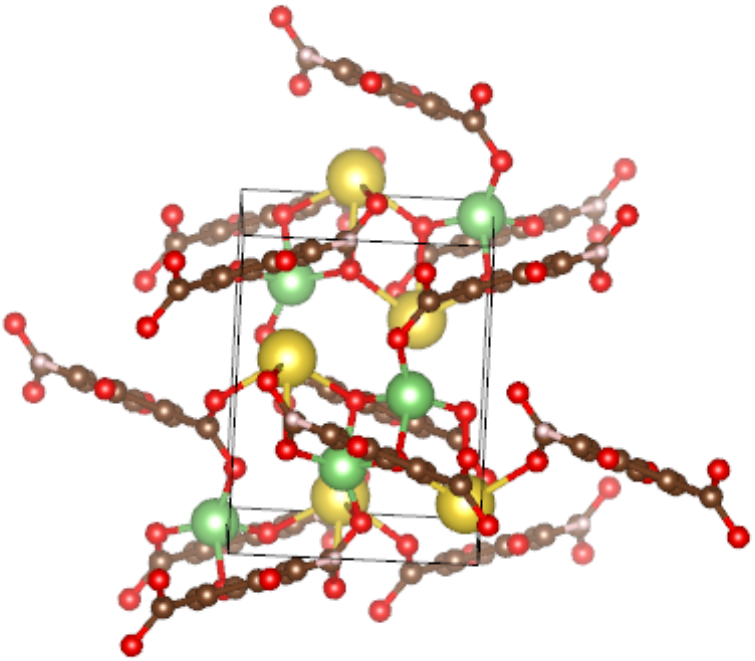

Figure 3.24: Predicted crystal structure for second lithiated phase of Na_2Li_2DHT. The color scheme is as in Figure 4.25

3.3.2 Voltage Profile

The lithiation process for the structures is:

$$Na_2DHT + 2Li^+ + 2e^- \rightarrow Na_2Li_2DHT$$

Similar to the electrode having a Calcium atom as an spectator cation, we calculated the internal energies using two methods. The first on being GGA-PBE and the second being the hybrid functional, HSE06. As for the electrode with the calcium atom, the energies of the hybrid functional are lower than the GGA-PBE ones. However, this difference does not pay an import role to the final calculated voltage. We found a calculated voltage of around 2.9 V, and the material has not been experimentally tested yet.

3.3.3 Electronic Structure

When it comes to the electrode having the sodium atom as a spectator cation, we see that the first filled band has a big contribution of the oxygen atoms bounded directly to the ring. Similarly to the previous electronic structure predictions, we see a big influence of the O group to the first band filled during first lithiation step. While, the second lithiation step is also filled majority by the COO groups and the aromatic ring.

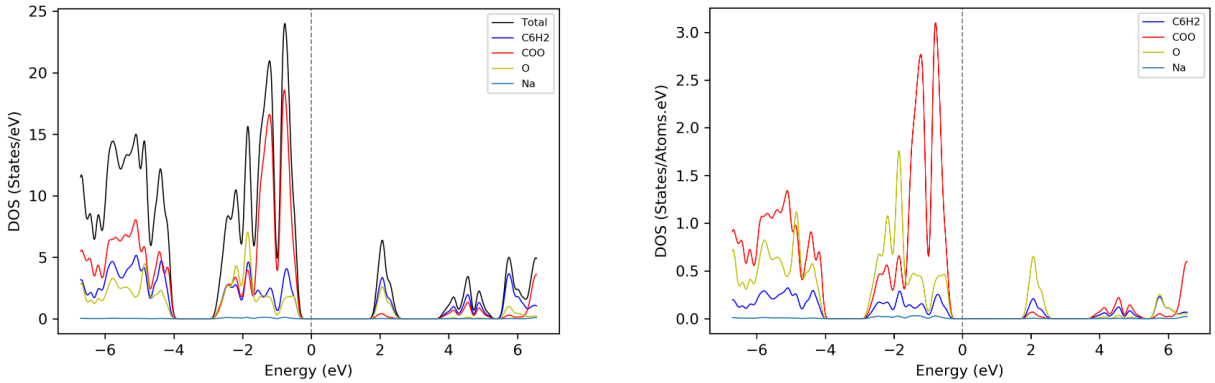

Figure 3.25: On the left: Density of States (DOS); on the right: Normalized Density of States (nDOS), of the delithiated phase Na_2DHT.

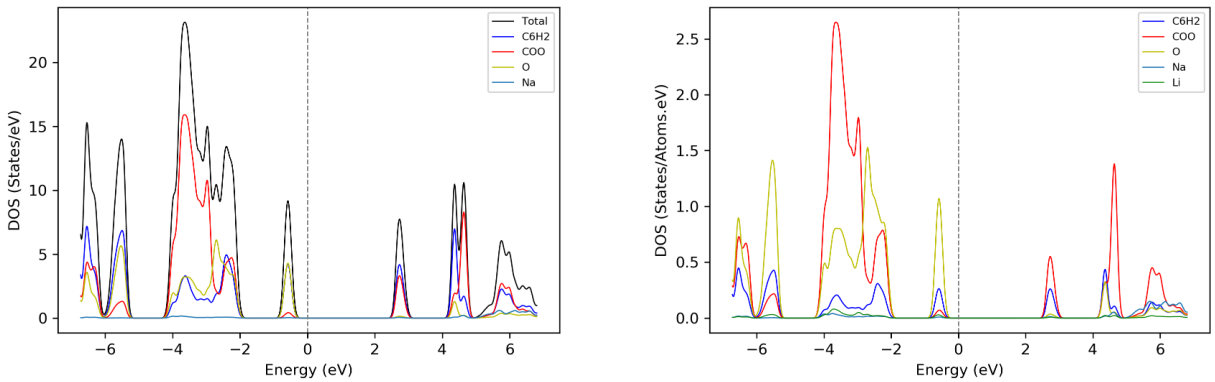

Figure 3.26: On the left: Density of States (DOS); on the right: Normalized Density of States (nDOS), of the Na_2Li_2DHT.

Figure 3.27 confirms our predictions on the dispersion of charge in the molecule. The aromatic ring is again working as a reservoir of charge and therefore shows the highest absolute gain of charge throughout the lithiation process.

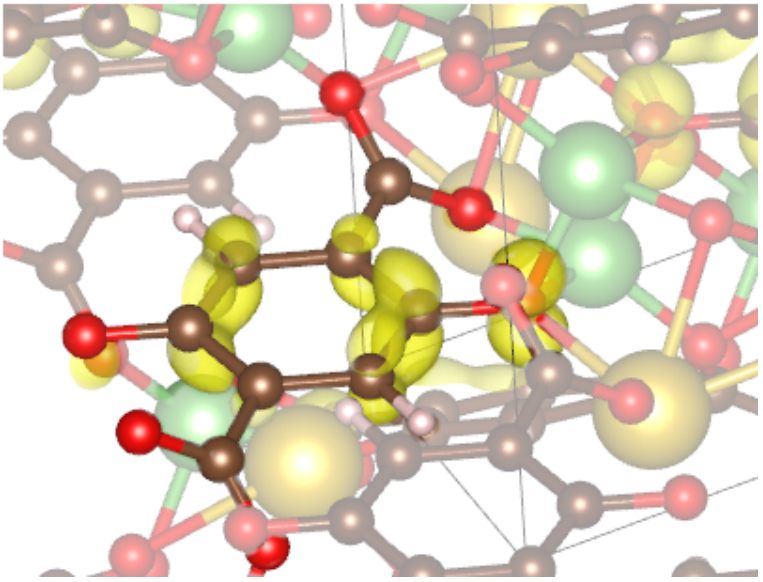

Figure 3.27: Charge density of the extra two electrons for Na_2Li_2DHT

3.3.4 Bader Charge Analysis

Until here, the discussion on the results for the sodium atom as a spectator cation have been really similar to the calcium atom. For the Bader analysis we represent two step lithiation, going from the delithiated stage to the second lithiation. Despite having really similar values to the redox potential of the calcium structure, the bader analysis reveals the change of the redox center in the molecule. While both the Ca and Na crystals shows the ring acting as a charge reservoir, the charge density here is higher on the O group than on the COO group.

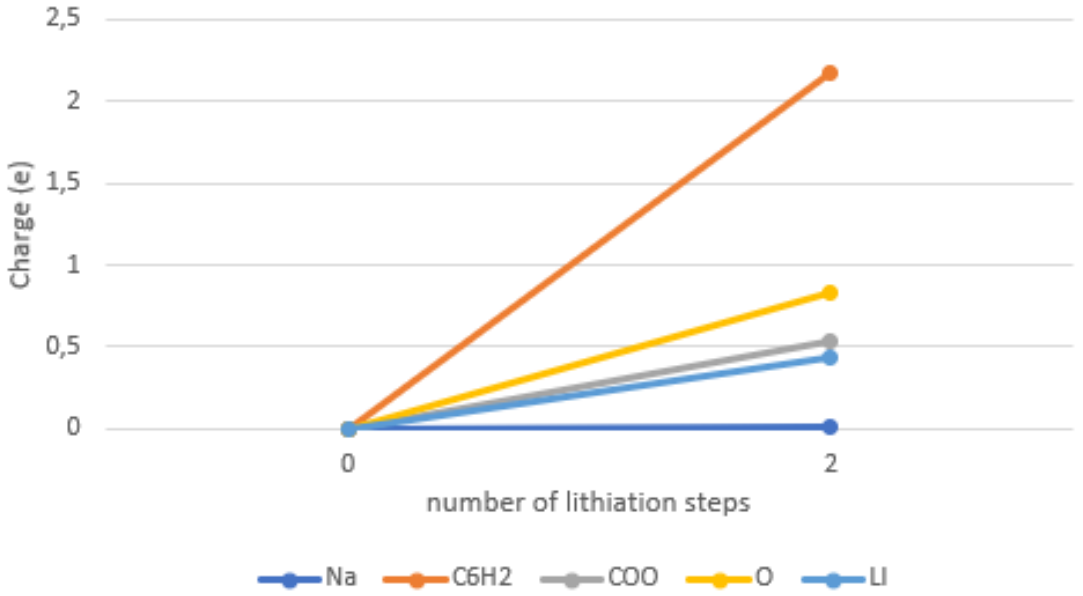

Figure 3.28: The Bader analysis results show a charge variation of each group present in the molecule as a function of the lithiation steps of the electrode

3.4 Discussion and Comparison

We found similarities in $MgLi_xDHT$ and $CaLi_xDHT$ crystal structures proposed by our USPEX calculations, they share similar features during the second step of lithiation, especially during the delithiated phase. On the other hand, Na_2Li_xDHT crystal structure is not as similar due to the different amount of spectator cations per molecule. Although having similar crystal structures, the electrode material with magnesium ions and calcium ions have notable different voltages after the second step of lithiation. While magnesium electrode shows a redox potential of 3.5 V, both calcium and sodium materials shows approximately 2.9 V value for the voltage. These results are with great agreement with experimental results, except the sodium as an spectator cation - to our knowledge, there is no experimental studies conducted for the material.

We further investigated higher lithiation steps for $MgLi_xDHT$. Results revealed a significant drop in the third litiation step, showing a 0.53 value for the voltage. Previous studies [45] [46] have shown organic anodes with voltage raging from 0.5 to 2.0, which indicates that the third litiation material can act as anode. Additionally, through our electronic and charge analysis, we found that the redox center changes

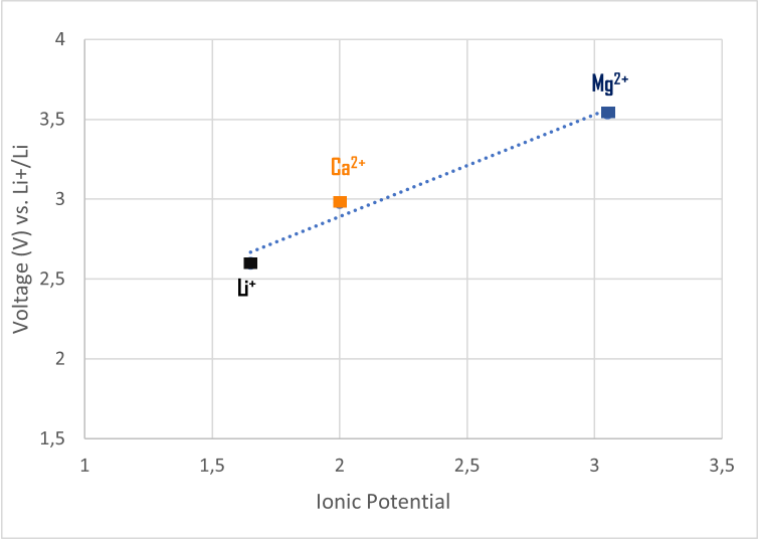

Figure 3.29: The comparison of the electrode voltages and ionic potentials.

from the O group to the COO group. In the DOS, we see the O band being filled first, and from the Bader analysis, we see the charge going from being more concentrated in the O group to being higher in the COO group. Interestingly, it has previously being shown that adding different groups and changing the redox center of a molecule can tune the voltage of an organic electrode [17].

Despite having similar redox potential values, the electrode with calcium and sodium ions show somewhat contrasting results. The Bader analysis implies that by the end of the second lithiation step, the charge variation is higher in the COO than in the O group for $CaLi_2DHT$. This result was unexpected and needs to be further investigated. While, for Na_2Li_2DHT, it is higher in the O group than in the COO group - notice both have the highest variation in the aromatic ring. DOS values, on the other hand, are to some degree similar. The results indicate that the first band filled is formed by the O, COO and the ring. However, the O group presents a higher density per atom for both materials.

Here, we conducted a study to predict the crystalline structures and some properties of XLi_2DHT organic electrodes, where X represents the different spectator cations. As far as we are aware, this is the first study that simulate and analyse these materials, without prior experimental input. Former studies have investigated other quinone-based electrodes through evolutionary algorithms implementation [16] [17] to predict the crystalline structure and properties of cathodes. Recently, machine learning meth-

ods are also being applied in the prediction of organic electrodes properties [47] [48] [49]. Thus, data driven methods together with evolutionary algorithms are likely to highly impact and accelerate new organic compounds discovery and prediction of their properties.

Besides proposing the structures and predicting the electrodes properties, the aim of this research was to analyse and bring light to the influence of the spectator cation in the molecule and their properties, initially studied experimentally by *Jouhara et al* [2]. It is beyond the scope of this study to certify the reason behind the voltage increase. Nonetheless, the data presented provide a new insight into this influence. For instance, the study implies that the correlation between the O group to a higher voltage. We then propose that the magnesium atom has a influence into the O groups, as also propose by [2]. Thus, further investigation is required to address this influence: properties as the electronegativity and ionic dispersion inside the electrode might also elucidate the investigation.

Chapter 4

Conclusions

In this research we aimed to study the influence of different spectator cations in the organic electrode material DHT. The use of Li-ion based electrodes is broadly commercial, however the understanding behind organic based electrodes are still overlooked. Nonetheless, we applied both DFT and the evolutionary algorithm based software, USPEX, to find possible crystalline structures and predict the electronic, charge and voltage profile for each lithiation step. As a result of this research, we could replicate and calculate the voltage profile of the $MgLi_2DHT$ electrode with great agreement to experimental results, without no previous experimental inputs. Therefore, we were able predict and extract important information of such materials.

Despite the remarkable advances, the state of the art for organic electrodes are still in disadvantage when compared to inorganic electrode materials. As studied [2], the $MgLi_2DHT$ material has outstanding properties for a OEM (organic electrode material) candidate. The main finding about it shows an increase of 800 mV when compared to the Li_2DHT, as also simulated by M. Alhanash [50]. As part of our findings we calculated the voltage for all the lithiated steps. A voltage of around 3.59 was found as the second lithiation step. Confirmed by the DOS and the charge profile, the O^- holds most part of the added electron density in the molecule. Our results also suggests the aromatic ring working as a charge reservoir.

In addition, we were also interested in predicting and investigating other spectator cations. The research extended to both both Ca and Na ions. Indeed, Ca also showed great experimental agreement. Based on the voltage profile and electronic structure,

the oxygen atom is still acting as the electron receptor. We investigated the Na cation with no previous studies in the literature. Moreover, we achieved a voltage profile similar to the $CaLi_2DHT$ to the second lithiation step of around 2.98 V. Although we found similar voltage profiles, there are intrinsic differences in the Bader charge analysis - that could be further investigated.

Here, we showed that the use of an evolutionary algorithm and other novel methods are relevant to study prospective and new electrode materials. In conclusion, we confirm the increase in voltage via cation substitution, as stated experimentally before; we obtained crystal structured predictions from USPEX, and, finally, we analysed different aspects of the materials to better understand the voltage increase.

Bibliography

[1] A. E. Lakraychi and A. Vlad, "Organic batteries-the route towards sustainable electrical energy storage technologies," *Chim. Nouv*, vol. 127, pp. 1–9, 2018.

[2] A. Jouhara, N. Dupré, A.-C. Gaillot, D. Guyomard, F. Dolhem, and P. Poizot, "Raising the redox potential in carboxyphenolate-based positive organic materials via cation substitution," *Nature communications*, vol. 9, no. 1, p. 4401, 2018.

[3] A. Jouhara, *De la conception de matériaux d'électrode organiques innovants à leur intégration en batteries" tout organique"*. PhD thesis, Nantes, 2018.

[4] J. Heyd, G. E. Scuseria, and M. Ernzerhof, "Hybrid functionals based on a screened coulomb potential," *The Journal of chemical physics*, vol. 118, no. 18, pp. 8207–8215, 2003.

[5] A. R. Huamantinco and H. M. Petrilli, "Estudo da superfície au (111) e da adsorção de'ch ind. 3 s'em au (111) através do método paw," 2003.

[6] A. E. Eiben, J. E. Smith, A. Eiben, and J. Smith, "What is an evolutionary algorithm?," *Introduction to evolutionary computing*, pp. 25–48, 2015.

[7] D. Larcher and J.-M. Tarascon, "Towards greener and more sustainable batteries for electrical energy storage," *Nature chemistry*, vol. 7, no. 1, pp. 19–29, 2015.

[8] J. Xie and Y.-C. Lu, "A retrospective on lithium-ion batteries," *Nature communications*, vol. 11, no. 1, p. 2499, 2020.

[9] A. K. Padhi, K. S. Nanjundaswamy, and J. B. Goodenough, "Phospho-olivines as positive-electrode materials for rechargeable lithium batteries," *Journal of the electrochemical society*, vol. 144, no. 4, p. 1188, 1997.

[10] M. M. Thackeray, W. I. David, P. G. Bruce, and J. B. Goodenough, "Lithium insertion into manganese spinels," *Materials Research Bulletin*, vol. 18, no. 4, pp. 461–472, 1983.

[11] D. Williams, J. Byrne, and J. Driscoll, "A high energy density lithium/dichloroisocyanuric acid battery system," *Journal of the Electrochemical Society*, vol. 116, no. 1, p. 2, 1969.

[12] T. B. Schon, B. T. McAllister, P.-F. Li, and D. S. Seferos, "The rise of organic electrode materials for energy storage," *Chemical Society Reviews*, vol. 45, no. 22, pp. 6345–6404, 2016.

[13] S. Lee, G. Kwon, K. Ku, K. Yoon, S.-K. Jung, H.-D. Lim, and K. Kang, "Recent progress in organic electrodes for li and na rechargeable batteries," *Advanced materials*, vol. 30, no. 42, p. 1704682, 2018.

[14] H. Chen, M. Armand, G. Demailly, F. Dolhem, P. Poizot, and J.-M. Tarascon, "From biomass to a renewable lixc6o6 organic electrode for sustainable li-ion batteries," *ChemSusChem: Chemistry & Sustainability Energy & Materials*, vol. 1, no. 4, pp. 348–355, 2008.

[15] H. Chen, P. Poizot, F. Dolhem, N. I. Basir, O. Mentré, and J.-M. Tarascon, "Electrochemical reactivity of lithium chloranilate vs li and crystal structures of the hydrated phases," *Electrochemical and solid-state letters*, vol. 12, no. 5, p. A102, 2009.

[16] C. F. Marchiori, D. Brandell, and C. M. Araujo, "Predicting structure and electrochemistry of dilithium thiophene-2, 5-dicarboxylate electrodes by density functional theory and evolutionary algorithms," *The Journal of Physical Chemistry C*, vol. 123, no. 8, pp. 4691–4700, 2019.

[17] R. P. Carvalho, C. F. Marchiori, D. Brandell, and C. M. Araujo, "Tuning the electrochemical properties of organic battery cathode materials: insights from evolutionary algorithm dft calculations," *ChemSusChem*, vol. 13, no. 9, pp. 2402–2409, 2020.

[18] J. Heiska, M. Nisula, and M. Karppinen, "Organic electrode materials with solid-state battery technology," *Journal of Materials Chemistry A*, vol. 7, no. 32, pp. 18735–18758, 2019.

[19] J. D. M. Vianna, *Teoria Quântica de Moléculas e Sólidos: simulaçao computacional*. Livraria da Física, 2004.

[20] M. Born and W. Heisenberg, "Zur quantentheorie der molekeln," *Original Scientific Papers Wissenschaftliche Originalarbeiten*, pp. 216–246, 1985.

[21] J. Kohanoff, *Electronic structure calculations for solids and molecules: theory and computational methods*. Cambridge university press, 2006.

[22] P. Hohenberg and W. Kohn, "Inhomogeneous electron gas," *Physical review*, vol. 136, no. 3B, p. B864, 1964.

[23] J. C. Slater, "The self consistent field and the structure of atoms," *Physical Review*, vol. 32, no. 3, p. 339, 1928.

[24] L. H. Thomas, "The calculation of atomic fields," in *Mathematical proceedings of the Cambridge philosophical society*, vol. 23, pp. 542–548, Cambridge University Press, 1927.

[25] E. Fermi, "Eine statistische methode zur bestimmung einiger eigenschaften des atoms und ihre anwendung auf die theorie des periodischen systems der elemente," *Zeitschrift für Physik*, vol. 48, no. 1-2, pp. 73–79, 1928.

[26] T. Tsuneda, "Density functional theory in quantum chemistry," 2014.

[27] W. Kohn and L. J. Sham, "Self-consistent equations including exchange and correlation effects," *Physical review*, vol. 140, no. 4A, p. A1133, 1965.

[28] C. C. J. Roothaan, "New developments in molecular orbital theory," *Reviews of modern physics*, vol. 23, no. 2, p. 69, 1951.

[29] P. A. Dirac, "Note on exchange phenomena in the thomas atom," in *Mathematical proceedings of the Cambridge philosophical society*, vol. 26, pp. 376–385, Cambridge University Press, 1930.

[30] J. P. Perdew and A. Zunger, "Self-interaction correction to density-functional approximations for many-electron systems," *Physical Review B*, vol. 23, no. 10, p. 5048, 1981.

[31] J. P. Perdew, K. Burke, and M. Ernzerhof, "Generalized gradient approximation made simple," *Physical review letters*, vol. 77, no. 18, p. 3865, 1996.

[32] A. D. Becke, "A new mixing of hartree–fock and local density-functional theories," *The Journal of chemical physics*, vol. 98, no. 2, pp. 1372–1377, 1993.

[33] M. Marsman, J. Paier, A. Stroppa, and G. Kresse, "Hybrid functionals applied to extended systems," *Journal of Physics: Condensed Matter*, vol. 20, no. 6, p. 064201, 2008.

[34] J. Paier, M. Marsman, K. Hummer, G. Kresse, I. C. Gerber, and J. G. Ángyán, "Screened hybrid density functionals applied to solids," *The Journal of chemical physics*, vol. 124, no. 15, p. 154709, 2006.

[35] A. D. Becke, "Density-functional thermochemistry. ii. the effect of the perdew–wang generalized-gradient correlation correction," *The Journal of chemical physics*, vol. 97, no. 12, pp. 9173–9177, 1992.

[36] P. E. Blöchl, "Projector augmented-wave method," *Physical review B*, vol. 50, no. 24, p. 17953, 1994.

[37] P. A. D. Petersen, *Cálculos ab initio de interações entre Cd e bases nitrogenadas do DNA*. PhD thesis, Universidade de São Paulo, 2011.

[38] C. W. Glass, A. R. Oganov, and N. Hansen, "Uspex—evolutionary crystal structure prediction," *Computer physics communications*, vol. 175, no. 11-12, pp. 713–720, 2006.

[39] P. A. Vikhar, "Evolutionary algorithms: A critical review and its future prospects," in *2016 International conference on global trends in signal processing, information computing and communication (ICGTSPICC)*, pp. 261–265, IEEE, 2016.

[40] M. Kumar, D. M. Husain, N. Upreti, and D. Gupta, "Genetic algorithm: Review and application," *Available at SSRN 3529843*, 2010.

[41] J. Hafner, "Ab-initio simulations of materials using vasp: Density-functional theory and beyond," *Journal of computational chemistry*, vol. 29, no. 13, pp. 2044–2078, 2008.

[42] V. S. Bagotsky, *Fundamentals of electrochemistry*, vol. 44. John Wiley & Sons, 2005.

[43] R. P. Carvalho, C. F. Marchiori, C. M. Araujo, and D. Brandell, "Atomic-scale modelling of redox-active organic molecules and polymers for energy applications," *Redox Polymers for Energy and Nanomedicine*, vol. 34, p. 93, 2020.

[44] W. Tang, E. Sanville, and G. Henkelman, "A grid-based bader analysis algorithm without lattice bias," *Journal of Physics: Condensed Matter*, vol. 21, no. 8, p. 084204, 2009.

[45] A. Eftekhari, "Low voltage anode materials for lithium-ion batteries," *Energy Storage Materials*, vol. 7, pp. 157–180, 2017.

[46] B. Esser, F. Dolhem, M. Becuwe, P. Poizot, A. Vlad, and D. Brandell, "A perspective on organic electrode materials and technologies for next generation batteries," *Journal of Power Sources*, vol. 482, p. 228814, 2021.

[47] R. P. Carvalho, C. F. Marchiori, D. Brandell, and C. M. Araujo, "Artificial intelligence driven in-silico discovery of novel organic lithium-ion battery cathodes," *Energy storage materials*, vol. 44, pp. 313–325, 2022.

[48] T. Lombardo, M. Duquesnoy, H. El-Bouysidy, F. Årén, A. Gallo-Bueno, P. B. Jørgensen, A. Bhowmik, A. Demortière, E. Ayerbe, F. Alcaide, *et al.*, "Artificial intelligence applied to battery research: hype or reality?," *Chemical Reviews*, vol. 122, no. 12, pp. 10899–10969, 2021.

[49] P. Friederich, F. Häse, J. Proppe, and A. Aspuru-Guzik, "Machine-learned potentials for next-generation matter simulations," *Nature Materials*, vol. 20, no. 6, pp. 750–761, 2021.

[50] M. Alhanash, "Effect of electronic exchange-correlation interaction in the physics of ion insertion in organic salts," 2021.